Jitte Jennekens, Bsc (6869718)
General Research Profile
Regenerative Medicine & Technology
Utrecht University

Melanoma-derived extracellular vesicles

Signaling through their miRNA content

Examiner: Prof. Dr. Richard Chahwan
Daily supervisor: Ala'a Al Hrout, Msc
Second examiner: Prof. Dr. Raymond Schiffelers

Internship conducted at Institute of Experimental Immunology,
University of Zurich

Utrecht, October, 2022

Abstract

Melanoma is the deadliest type of skin cancer. Early diagnosis is of great importance for patient outcome. Currently, genetic testing is required to determine the mutational background. Promising research on extracellular vesicles (EVs) could offer a potential new method to diagnose melanoma. Melanoma cells are known to secrete these EVs as an oncogenic signaling mechanism. One of the components packaged in EVs are miRNAs. It was hypothesized that melanoma mutants BRAF, NRAS, and double mutant distinctively regulate the miRNA composition in secreted EVs. Identifying this mutant-specific miRNA profile in the blood of patients could be used to diagnose melanoma and the mutation. To test whether EV-enriched miRNAs are melanoma-mutant dependent, and whether these signature miRNAs also alter gene expression in recipient cells, we compare the miRNA profiles of EVs and their cellular counterparts for different melanoma mutant cell lines (BRAF, NRAS, double mutant). Target prediction and in vitro target validation is performed to elucidate the regulatory role of these candidate signature miRNAs. We show that EV miRNA profiles are distinct from their matched cellular profiles. The signature miRNA identified for BRAF mutant melanoma cell lines, hsa-mir-6728-3p, enhances TGF-beta signaling via ITCH and Smad2/3 phosphorylation. TGF-beta signaling is known to promote tumorigenesis, drug resistance, and immune surveillance in melanoma. In addition to target validation, we aimed to shed light on miRNA sorting mechanisms in EVs. The existing hypothesis of selective miRNA sorting is based on the specific recognition of motifs within the miRNA sequence by sorting proteins. In our miRNA dataset, such sorting motifs could be identified in the EV-enriched miRNAs and cell-retained miRNAs. Although sorting motifs are highly cell line dependent, some of the identified motifs were shared between the melanoma cell lines and also between previously identified motifs by others, suggesting a conserved nature. Interestingly, these motifs are located primarily at the 3’ end of the miRNA sequences. Altogether, we identified a signature miRNA for BRAF and double mutant melanoma cell lines. For the BRAF signature miRNA we were able to show its capability to regulate the TGF-beta pathway, underlying the importance of EV-miRNAs in tumorigenesis. Sorting of miRNAs into EVs is an extremely complex mechanism that is highly cell line dependent. Our data suggest, in line with previous literature, the existence of sorting motifs within the miRNA sequences.

Layman's summary

Melanoma is an aggressive type of skin cancer and its incidence has been rising over the years. Early diagnosis is crucial, because successful treatment becomes increasingly difficult with later stages of the cancer. To determine the appropriate treatment, it is necessary to know if changes in certain genes have occurred. For example, half of the melanoma patients have a mutation in the BRAF gene. This can be determined by examination of a small piece of tissue removed from the tumor, called a biopsy. Research is focusing on finding new and less invasive methods to more easily diagnose melanoma. One potential method that has received a lot of attention is looking at extracellular vesicles (EVs), which are particles released from all cell types in the body. These EVs are released from cells and can end up in our blood. Since they carry information about the cells that secreted them, this can be used for the diagnosis of cancer. For example, in patients with melanoma, these EVs could carry information about the mutation of the cancer cells. In this report we specifically look into one of the types of cargo these EVs carry, called miRNAs. miRNAs are short sequences known to inhibit processes in cells. Research has shown that cancer cells secrete different miRNAs than healthy cells. In this study, we look at the miRNAs in these EVs secreted by melanoma cell lines with different mutations (BRAF, NRAS, and double mutant). We aimed to identify specific miRNAs that are present in the EVs from all cell lines with the same mutation, but not in the EVs from cell lines with the other mutations. We called these miRNAs signature miRNAs. Next, the function of these signature miRNAs is studied by looking at its potential targets. For one of the signature miRNAs for the BRAF mutant cell lines we were able to identify the TGF-beta pathway as a target. This target was predicted by an online tool and validated with experiments. Another question we wanted to answer in this report is how certain miRNAs get packaged into these EVs while others remain in the cells. Therefore, we looked at the sequences of the miRNAs consisting of ~20 nucleotides. It was hypothesized that the miRNAs that were sorted into EVs all shared a short motif within the sequence which determined their export. We were able to identify these sorting motifs for all cell lines with an online tool. Our data show that for each cell line, multiple motifs exist. In addition, they differ per cell line. This shows how complicated the process of miRNA sorting into these EVs is. More research is necessary to further understand the mechanisms.

Abbreviations

3D	Three-dimensional
miRNA	microRNA
UV	Ultra violet
EV	Extracellular vesicles
UTR	Untranslated region
TME	Tumor micro-environment
hsa-mir	Homo Sapiens miRNA
P/S	Penicillin-Streptomycin
FCS	Fetal Calf Serum
SD	Standard deviation

Contents

Introduction

Melanoma epidemiology

Melanoma is a cancer originating from melanocytes. These neural crest-derived cells produce melanin and are located in the basal layer of the epidermis. Dysregulation in melanocytes can give rise to phenotypically and genetically distinct melanocytic neoplasms ranging from benign lesion to malignant melanomas (1). The type of melanoma depends on ethnicity, lifestyle and genetic background of the patient. The most common type is cutaneous melanoma (2). Although accounting for only 1% of all skin cancers, melanoma is the most fatal, responsible for 80% of skin cancer deaths (3,4). Exposure to UV radiation is a major risk factor for this cancer type. Over the past decades the incidence has been rising and is expected to continue to increase. This creates both a burden on our health care system associated with tremendous costs as well as a significant clinical problem. Ongoing research is indispensable in order to develop new and improved methods for diagnosis and treatment.

Mutations in melanoma

Melanocytes not only reside in the skin but also throughout the body in uveal, mucosa, inner ear and rectum. Melanoma can occur in all locations where melanocytes reside, but skin cancer is the most common. Their main function is producing melanin to protect against photodamage. Melanocytes deliver this melanin to neighboring keratinocytes providing a layer of protection against UV radiation-induced DNA damage (5). In addition to environmental risk factors, genetic factors are a major contributor to the pathogenesis of melanoma (familial and sporadic melanoma). Familial genetic predisposition accounts for only 3-15% of melanomas, whereas somatic mutations represent the largest subset of melanomas. The major somatic mutations found in melanomas include BRAFV600E mutation found in approximately 60% of melanomas and NRAS mutations found in 15%-20% of melanomas (3). These mutations are UV-independent but often require additional mutations resulting from UV exposure in order to drive malignant transformation of melanocytes (6,7). BRAF and NRAS mutations are known to induce hyperactivation of the MAPK pathway in melanocytes. This signaling pathway regulates cell proliferation, growth, and migration (8,9). In short, the pathway is activated upon binding of a ligand to a tyrosine kinase receptor. This triggers activation of RAS family members and subsequent serial cascade activation of serine/threonine kinases. Phosphorylation of ERK, leading to its activation, activates its target transcription factors, thereby regulating gene expression.

BRAFV600E mutation is characterized by the substitution of valine into glutamate as a result of the transversion of a thymidine into adenine (T → A). Constitutive activation resulting from NRAS mutations and subsequent activation of its downstream targets will, similar to BRAF mutations, lead to uncontrolled cell growth and proliferation. In contrast to a BRAF mutation, NRAS mutations not only hyperactivates the MAPK pathway but also the PI3K pathway (10,11). BRAF and NRAS mutations are mutually exclusive, meaning that on a single-cell level they cannot occur concomitantly, due to self-induced apoptosis upon continuous MAPK hyperactivation. However, double mutants are rarely reported (12). BRAF and NRAS mutations are driver-mutations in melanoma. These gain of function mutations initiate the oncogenic events in melanocytes and melanocytic neoplasms formation. Progression to subsequent stages is characterized primarily by loss of function mutations in tumor-suppressor genes such as TP53, NF1, RAC1, CDKN2A, and PTEN.

Melanoma treatment

Deciphering the pathogenesis and disease progression of melanoma has benefited its treatment tremendously (13). For patients diagnosed with early-stage melanoma, surgical excision is the primary treatment and can be curative in the majority cases. Treating more advanced stages of melanoma remains challenging, even though the outcome for these patients has been transformed revolutionary in the past decade with advances in immune checkpoint inhibitors (anti-CTLA4 and anti-PD1) and targeted therapy (RAF and MEK kinase inhibitors) (14). Patients with a BRAF mutation have been shown to benefit most from a combination of BRAF and MEK inhibitors with or without immune checkpoint inhibitors. In response to treatment with BRAF/MEK inhibitors, although they prolong life, patients inevitably develop acquired drug resistance. One of the proposed mechanisms is that melanoma cells acquire an additional NRAS mutation. BRAF and NRAS mutations are thought to be mutually exclusive, however, resistant tumors that acquire both mutations may be comprised of multiple subclones containing either the NRAS or BRAF mutation. Double BRAF/NRAS mutations have also been shown to co-occur on a single-cell level in patients with acquired drug resistance (12).

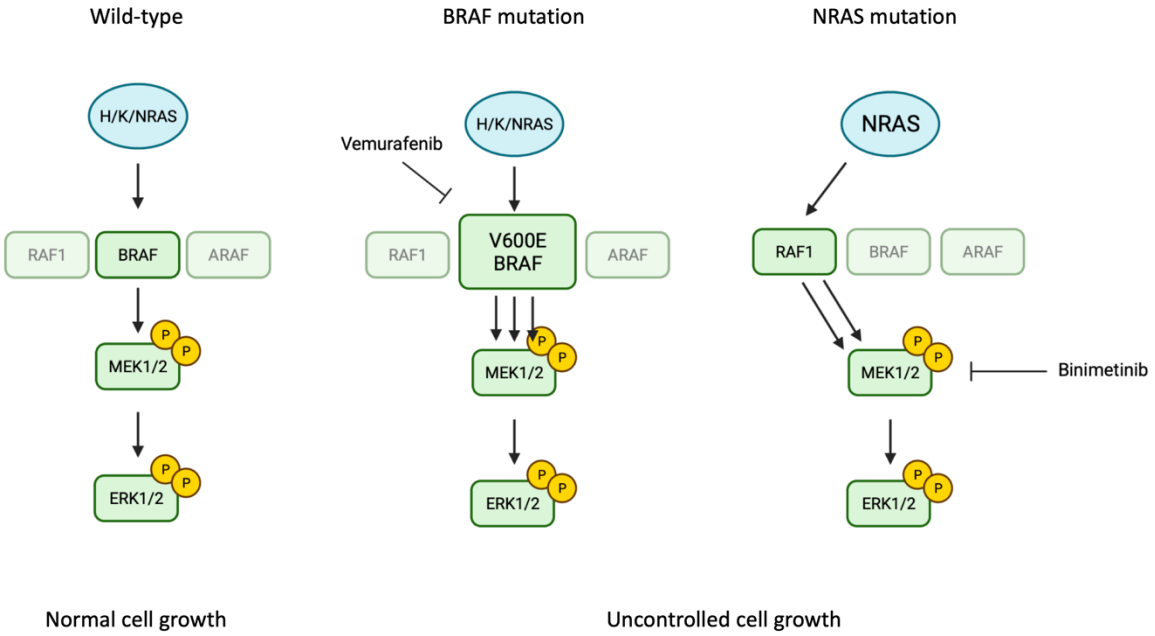

Figure 1. The MAPK pathway in Melanoma. The left panel shows the MAPK pathway for Wild-type melanoma without any mutations. MAPK pathway activation in wild-type melanoma mainly signals through the BRAF kinase and will stimulate normal cell growth. In the middle panel, the MAPK pathway is shown for melanoma with a BRAF mutation. The BRAFV600E mutant will lead to increased downstream activation of MEK1/2 and ERK1/2. Vemurafenib is used as a targeted therapy to inhibit the mutated form of BRAF and thereby inhibiting downstream pathway activation. The right panel shows the MAPK pathway for melanoma with an NRAS mutation. This mutant causes isotype switching from BRAF to RAF1 and subsequent increased pathway activation via MEK1/2 and ERK1/2. Melanoma with NRAS mutations is treated with MEK1/2 inhibitors such as Binimetinib. Both BRAF (middle) and NRAS (right) mutations cause uncontrolled cell growth.

Extracellular vesicles and melanoma

Early diagnosis is a key parameter for patient survival. Currently, diagnosis is based on histology, the visual observations of the clinician for staging of the tumor, and genetic testing to decide on treatment (15). To improve diagnosis of melanoma, biomarkers, defined as constituents of body fluids or tissues, could play an important role. Identifying biomarkers for diagnosis or monitoring of treatment effectiveness has received great attentions in research in the past decades, especially in the context of cancer. With the rapidly growing incidence of melanoma, new approaches for non-invasive and early diagnosis are needed in order to reduce mortality. One of these approaches might be the detection of tumor-derived components in the

circulation. A substantial amount of research has shown that components of tumors that are shed into the circulation, can be detected in liquid biopsies. One of these components that end up in the circulation are miRNAs encapsulated in extracellular vesicles (EVs). Extracellular vesicles are membranous structures that can be secreted by all cell types. This mechanism has been observed in organisms from bacteria to human. Being conserved throughout evolution underlines the biological importance of EVs. At first it was thought, that secretion of EVs was simply a mechanism for cells to dispose of unneeded compounds. Recently it became commonly accepted that EVs are not just waste carriers but rather play an active role in cellular communication. This novel mode of cell-to-cell communication is based on transfer of the EV content from a donor cell to a recipient cell and consequently affect gene regulation in this target cell. This discovery has led to a shift in focus towards their capacity to participate in cellular signaling in a normal and pathological state. Extracellular vesicles is the generic name used to describe a heterogenous group of cell-derived membranous vesicles. Because of their small and variable size (ranging from 50nm to 1um) characterization was difficult. EVs are now generally classified into exosomes (50-150nm) or microvesicles (50-500nm). Exosomes are from endosomal origin whereas microvesicles derive from the plasma membrane. Research has identified different types of cargo within these EVs, including proteins, lipids and nucleic acids (DNA sequences, mRNAs, and non-coding RNAs) which can highly vary between cells. The specific content of EVs directly affects its function once taken up by recipient cells, supporting the theory of precisely regulated cargo sorting.

miRNAs and melanoma

One of the best studied molecules that can be found in EVs are microRNAs (miRNAs). These small non-coding RNAs are processed from pre-miRNA into mature miRNA sequences (20-22 nucleotides). miRNAs are primarily known to negatively affect gene expression by targeting mRNA sequences. Binding of miRNAs and thereby inhibiting or triggering degradation of mRNA occurs on the 3' UTR of the mRNA sequences. A miRNA binds the 3'UTR region with a seed region located at the 5' end of the miRNA sequence. This interaction is not fully complementary and allows for mismatches in the binding. Therefore, one miRNA can have multiple targets. This mechanism of gene expression regulation is important in the context of cancer, as studies have shown altered miRNA expression levels contributing to tumor initiation and progression (16-18).

As we known now, these miRNAs not only regulate gene expression intracellularly but can also target cells in their local or distal environment. miRNAs can be packaged into EVs which are excreted from cells (19,20). However, the mechanism behind the specific sorting of miRNAs into EVs remains largely unknown. Previous studies have reported short tetranucleotide sequences within the miRNA sequence to which sorting proteins could bind, suggesting specific motifs could trigger sorting into EVs (21-25). But, conclusive evidence is lacking. Similarly, what determines which miRNAs stay inside the cell of origin remains unknown. The current hypothesized mechanism is based on the recognition of short motifs within the miRNA sequences by proteins, which subsequently sort the miRNAs into EVs. (figure 2)

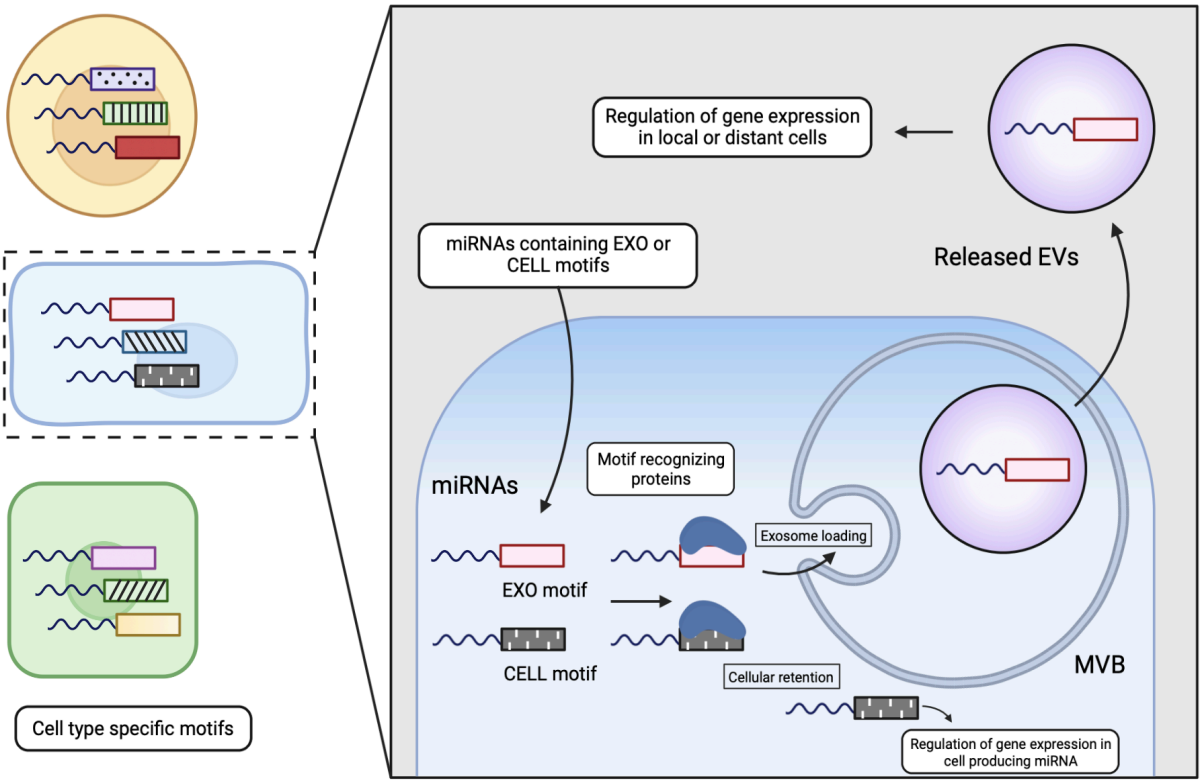

Figure 2. Proposed mechanism of miRNA sorting. The current hypothesis of miRNA sorting is based on motifs within the sequence of miRNAs. These sequences can be recognized by sorting proteins in the cell that either sort a miRNA into EVs or retain them in cells. Different cell types express different miRNAs. Motifs can differ between miRNAs and thus between cell types. Depending on the sorting proteins available in that specific cell type, miRNAs are distributed.

Previous research has shown that cancer cells secrete higher amounts of EVs and EV-encapsulated miRNAs, which can be detected in the circulation. This altered miRNA secretion in EVs provides the opportunity to be identified as novel diagnostic markers (26). In this report miRNA sequence data derived from either EVs or cells from melanoma spheroids was used to identify important miRNA regulators for the specific cell lines. It was hypothesized that cell lines from the same mutants might share signature miRNAs specific to that mutant. Target prediction and subsequent downstream target validation of these candidate miRNAs was performed to identify their regulatory role in these melanoma cell lines. Based on the miRNA sequence data, motifs were identified for either EV-enriched miRNAs or cell-retained miRNAs to provide an argumentation how these specific sets of miRNAs could be sorted into EVs.

Materials and Methods

Culture of melanoma cell lines
In this study, patient-derived melanoma cell lines with different mutations (BRAF, NRAS, and double mutant) were cultured. Cell lines were obtained from URPP biobank Zurich and maintained in RPMI-1640 media (Sigma-life-sciences) supplemented with 5% Penicillin-Streptomycin (P/S; Gibco) and 10% Fetal Calf Serum (FCS; Gibco). Cell were seeded in standard T25 culture flasks and passaged twice a week. Briefly, at 90%-100% confluency, cells were washed with PBS followed by incubation with TryplE (Gibco) for 3 minutes at 37°C. After dissociation, the cultures were collected and spun at 300xg for 5 minutes. Supernatant was removed and cells were resuspended in RPMI-1640 media supplemented 5% P/S 10% FCS and split 1:2 into a new T25 flask. If cells were seeded for an experiment, the cells were counted and seeded with the required seeding density. Cells were counted with a hemocytometer under the microscope using trypan blue (Gibco).

Spheroid formation
For experiments in a 3D setting, cells were cultured as spheroids in ultra-low attachment cultureware. In a 96-well plate (Corning Spheroid microplate 96-well; Ultra-low attachment), 1000 cells/well were seeded in 100ul of RPMI-1640 media supplemented 5% P/S and 10% FCS. In a T175 (Corning; Ultra-low attachment) three million cells were seeded in 15ml of RPMI-1640 media supplemented 5% P/S and 10% FCS. Spheroids cultured in a T175 were transferred to a standard 12-well plate after three days of culture for subsequent antagomir treatment experiments. Spheroids were maintained for 5-6 days depending on the experiment.

Drug treatment
The BRAFV600E inhibitor Vemurafenib (MedChemExpress) and MEK1/2 inhibitor Binimetinib (MedChemExpress) were used in this study. The drug was resuspended in DMSO (PAN-Biotech) and diluted with PBS accordingly. First, the IC50 was determined for both drugs. BRAF cell lines were treated with Vemurafenib and Double mutant cell lines were treated with both Vemurafenib and Binimetinib. Spheroids were treated on day 3 with different concentrations and cell viability was assessed on day 6. Drug doses ranged from 10nM to 20uM for the BRAF cell lines M111031, M150506, and M150536 and 1uM to 20uM for the double mutant cell lines M140906 and M121224. For subsequent drug treatment experiments spheroids were treated with 10uM of the drug Vemurafenib based on the IC50 curve.

Antagomir miRNA silencing experiments
Antagomirs were selected for the specific melanoma mutants, hsa-mir-6728-3p for BRAF and hsa-mir-6836-3p for double mutant based on their signature expression in these mutants. After resuspension in Tris-EDTA buffer (Fisher Bioreagents), antagomirs were administered in either a 2D or 3D setting on day 3 with a concentration of 100nm, 700nm, or 1uM. Cells were harvested 2 days after antagomir incubation. A negative control antagomir (Qiagen; Negative control A) was used as control.

Viability assay
Cell viability was assessed with CellTiter-Glo 3D Cell Viability Assay according to the manufacturer's protocol. In short, cells were treated with the CellTiter-Glo® 3D Reagent in the same volume as the culture volume. Cells were put on the shaker for 15 minutes to induce lysis and incubated another 15 minutes in the dark to stabilize the detection luminescence.

Luminescence assay was performed on a TECAN infinite M Plex with an integration time of 1000ms. Viability was calculated as percentage of the untreated control.

Microscopic imaging
Representative Bright field images were taken of the spheroids on multiple timepoints for the duration of the experiments. Transfection efficiency of the labeled antagomirs was determined with fluorescent microscopy (Leica DFC7000T).

Western blot
Spheroids were collected and subsequently lysed with RIPA buffer containing phosphatase and protease inhibitor and incubated on ice for 30 minutes. The samples were spun down at 12000xg for 30 min at 4°C degrees. Supernatant was collected and BCA was performed to determine protein concentration with the Pierce™ BCA protein assay kit (Thermo Fischer) according to the manufacturer's protocol. For the western blot, 20ug protein was loaded into a 4-20% gel (Witec AG) with 1X loading buffer. Prime-Step Prestained Broad Range Protein Ladder (Biolegend) was used to estimate protein molecular weight. The gel ran at a constant 80V until the samples left the stacking gel. Then, voltage was increased to 120V until the samples reached the bottom of the gel. Protein was transferred with a Trans-Blot Turbo Transfer System (Bio-Rad) from the gel to a blot (50min; 12.5V; 0.5A) in transfer buffer (Supplementary table 1). After transferring, the blotting membrane was blocked for 1h in 5% BSA (Chemie Brunschwig AG/ pan biotech) at RT on a shaker. Subsequently, the membrane was cut according to the protein bands of interest. Blots were incubated over night at 4°C degrees in the dark with the appropriate antibody dilutions (supplementary table 2). After primary incubation, blots were washed 3x for 5-10min with TBST (Supplementary table 1). Next, the corresponding secondary antibody was added and incubated for 1h at RT (supplementary table 2). Blots were washed again 3x for 5-10min with TBST. Visualization was done with a chemiluminescent signal and an exposure time of 30s-1min. Blots were stripped with a mild-stripping buffer (Supplementary table 1) and restaining with primary and secondary antibodies to allow the analysis of more proteins on the same blot. The western blot images were quantified using ImageJ. Protein expression levels were normalized to the housekeeping control and plotted as relative protein expression compared to the negative control.

Bioinformatic analysis
The miRNA sequences of the miRNA data set were analyzed to investigate potential sorting mechanisms. The miRNA read counts determined from the sequence data from either EV or Cellular samples was grouped into either EV-enriched, cell-retained, or not enriched. miRNAs in EVs with a read count of >2 and a fold-enrichment (FE), defined as the ratio between read count in EV and read count in cell sample, of >3 were considered EV-enriched. miRNAs with a read count of >3 in cells and no read counts in EVs were considered cell-retained miRNAs. The rest of the miRNA data set was considered not enriched. EV-enriched and cell-retained miRNAs were compared between cell lines from the same mutant to identify signature miRNAs.

The percentage of the CG base pairs in the miRNA sequences was determined in Benchling. GraphPad was used to plot the CG percentage of EV-enriched vs cell-retained miRNA and statistical significance was determined. miRNA motif enrichment was performed using the free online available tool STREME. This software allows users to upload both input sequences and control sequences. The tool will then discover motifs that are enriched or relatively enriched in your input sequences compared to the control sequences. Motifs were discovered for either EV-enriched miRNA sequences or cell-retained sequences. Length of the motifs was set at 4-7 base

pairs. Sequences were aligned on their centers, which is the default setting of the software. From the discovered motifs, only the motifs with 0% occurrence in the control sequences and an E-value of >0.05 were selected. Next, from these 'extended sequences' the core sequence was determined by identifying the core sequences with the highest occurrence in the input sequences. For the core sequences the percentage in input and control sequences was determined and the resulting fold-enrichment. Location of the motifs in these sequences was plotted in GraphPad as either occurring in the first half of the miRNA sequence (base pair 1 - 9) or the second half of the miRNA sequence (base pair 10 - 3'-end).

Statistical analysis

GraphPad Prism software (version 9.3.1) was used to calculate statistical significance by unpaired t-testing. Data values represent the means and the error bars represent the standard deviation (SD). To indicate p-values, the following convention is used: * = $p < 0.05$, ** = $p < 0.01$, *** = $p < 0.001$.

Results

Clustering of Cell samples vs EV samples

Previously generated miRNA sequencing data in the lab was used for the bioinformatic analysis of the miRNA profiles of EVs and their cellular counterparts. From 12 melanoma cell lines with different mutation backgrounds (4x BRAF, 4x NRAS, 4x double mutant), EVs were isolated. From the EVs and their corresponding cells of origin, RNA was isolated and sequenced (figure 3). One BRAF and one NRAS cell line were excluded from analysis because of low read counts. The miRNA profiles are visualized in a heatmap (figure 4). Hierarchical clustering of both rows and columns shows samples primarily cluster based on sample type (EV vs cell), suggesting that EV miRNA profiles differ from cellular miRNA profiles. Regarding genomic background, the clustering is less pronounced. As expected, samples from double mutant cell lines also cluster with BRAF and NRAS mutants, since double mutants contain both BRAF and NRAS mutations. Principal component analysis (PCA) of cellular and EV miRNAs separate shows that cluster can be identified based on their mutation, suggesting the different mutations might be associated with the secretion of specific miRNAs. The EV miRNA profiles were, therefore, used to identify mutant specific signature EV-miRNAs. The regulatory role of these candidate miRNAs was subsequently validated in vitro.

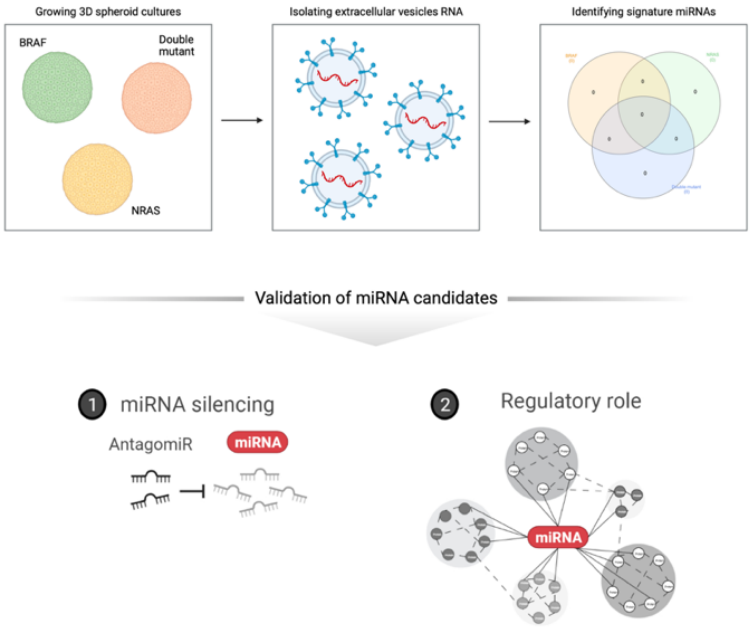

Figure 3. **Graphical schematic of the experimental set up.** RNA was isolated from the spheroids and their EVs of three different melanoma mutants. Based on the sequencing data, signature miRNAs were identified for the specific mutants. The regulatory role of these candidate miRNAs was validated in vitro with antagomir experiments and literature review.

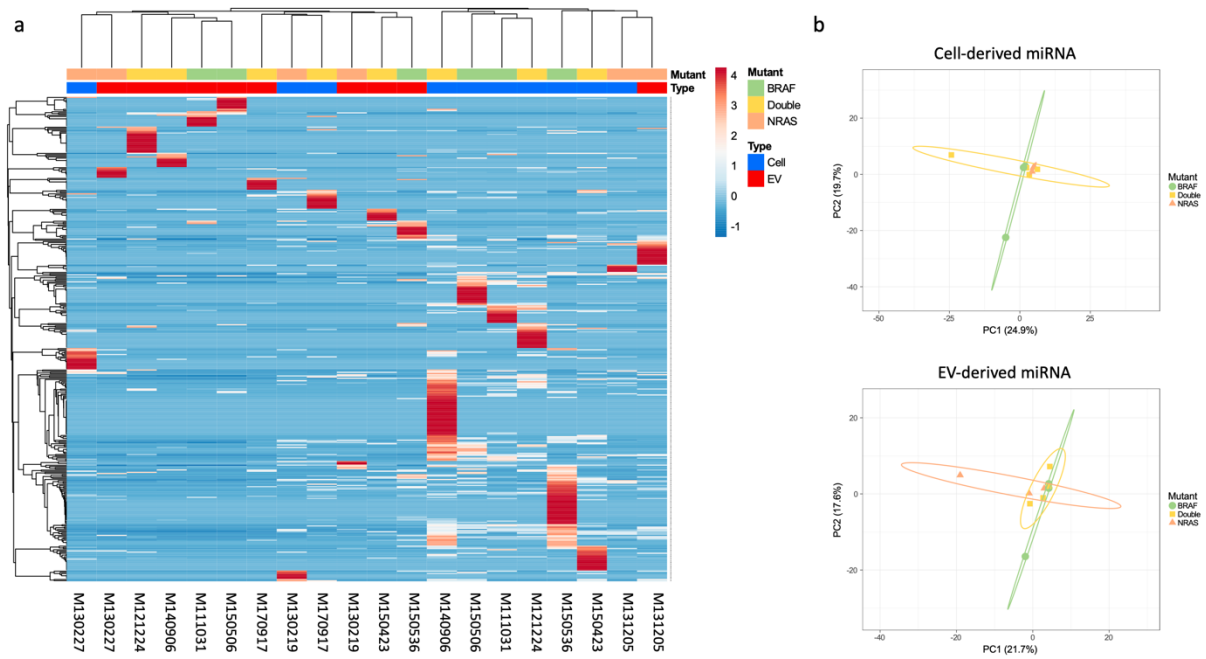

Figure 4. Cell-derived vs EV-derived miRNA profiles a) Heatmap of the miRNA profiles of EV and cell samples for 10 melanoma cell lines. Rows are centered; unit variance scaling is applied to rows. Both rows and columns are clustered using correlation distance and average linkage. 359 rows, 20 columns. Sample type (Cell=blue; EV=Red) and mutation (BRAF=green; Double mutant=yellow; NRAS=orange) are indicated above. Cell line is indicated below. b) PCA plots of cell-derived miRNA profiles and EV-derived miRNA profiles. Mutation (BRAF=green; Double mutant=yellow; NRAS=orange) is indicated on the right. Unit variance scaling is applied to rows; SVD with imputation is used to calculate principal components. X and Y axis show principal component 1 and principal component 2 that explain 19.7% and 24.9% of the total variance for cell-derived miRNA and 17.6% and 21.7% of the total variance for EV-derived miRNA, respectively. Prediction ellipses are such that with probability 0.95, a new observation from the same group will fall inside the ellipse. N = 10 data points for each PCA plot.

BRAF and Double mutant specific signature miRNAs

Melanoma-derived circulating EVs containing mutant specific miRNAs could provide a great opportunity to improve diagnostics. For BRAF and double mutations, miRNAs that were expressed in at least two cell lines from that mutant were identified using Venn diagrams (supplementary figure 1). The resulting list of candidate miRNAs for these mutants (supplementary figure 1) was crosschecked with available literature. However, validated targets and knowledge about their regulatory role was lacking for all miRNAs. For the BRAF mutation hsa-mir-6728-3p, expressed in EVs from cell lines M111031 and M150506 was selected for subsequent in vitro validation. For the double mutants hsa-mir-6836-3p, expressed in cell lines M121224 and M140906 was selected for subsequent in vitro validation experiments. Criteria for selecting these miRNAs from the list of candidates included a high read count in EVs and no expression in cell lines from other mutations. First, the downstream regulatory role of hsa-mir-6728-3p (BRAF signature) was validated. Since there were no known targets for these candidates a target prediction analysis was performed. Three free online available tools for miRNA target prediction (TargetScan, DIANA, miRDB) were used and compared (supplementary figure 2). From the overlapping list of predicted targets, the TGF-beta pathway was identified to be the most enriched (z-score=3.26; 28 of genes overlapped). Interestingly, TGF-beta signaling is known to be important cancer. It is a well-studied pathway with regard to tumorigenesis and it has a known role in immune inhibition, drug resistance, and regulating the TME in melanoma. Therefore, this pathway was pursued in in vitro experiments.

Silencing of hsa-mir-6728-3p does not alter cell viability and drug sensitivity of BRAF mutant melanoma cells

The TGF-beta pathway has a known role in cell growth and drug resistance in melanoma. It was hypothesized that BRAF signature miRNA hsa-mir-6728-3p could regulate cell viability drug resistance in melanoma via the TGF-beta pathway. Firs, the IC50 curve for BRAFV600E inhibitor Vemurafenib was established. Spheroids from the three BRAF cell lines (M111031, M150506, and M150536) were treated with increasing concentrations of the drug ranging from 1nm to 20uM. A schematic timeline of the experimental set up is shown in figure 5a. Representative images of the spheroids before drug treatment (day 3) and after drug treatment (day 6) are shown in figure 5b. Viability of the spheroids at day 6 after 72 hours of drug treatment is plotted in figure 5c. The number of technical replicates is indicated with an n and the number of experiments for each dose is indicated by the letter s. M111031 and M150506 form dense spheroids. By contrast, M150536 remains a lose cluster of cells. The lowest dose of 10nm does not seem to affect cell viability in these BRAF spheroids. The largest reduction in cell viability occurs with a dose of 20uM. M111031 decreases in viability from 78% at 10uM to 54% at 20uM. M150506 decreases in viability from 53% at 10uM to 16% at 20uM. M150536 decreases in viability from 65% at 10uM to 23% at 20uM. For subsequent experiments with Vemurafenib in BRAF cell lines, a dose of 10uM was used to study the effect of hsa-mir-6728-3p on drug resistance.

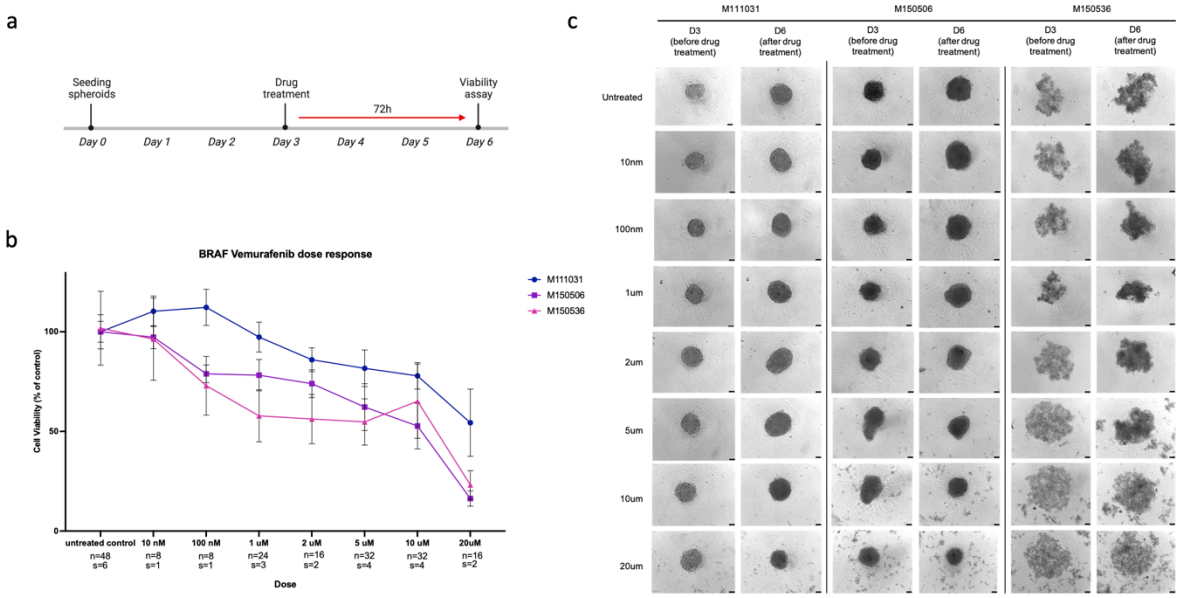

Figure 5. Vemurafenib dose response BRAF cell lines. a) Schematic of the experimental set up. Spheroids were seeded on day 0 and treated on day 3 with Vemurafenib for 72h. On day 6 cells were harvested for cell viability assay. b) Graph of BRAF cell lines dose response to Vemurafenib. For the different Vemurafenib doses, cell viability as percentage of control is plotted for the three BRAF cell lines. M111031 in blue, M150506 in purple, and M150536 in pink. n = number of replicates and s = number of experiments included each dose. SD is indicated by the error bars. c) Representative bright field images (10X magnification) of spheroids from three BRAF cell lines (M111031, M150506, M150536) on day 3 before drug treatment and on day 6 after 72h of drug treatment for different doses of Vemurafenib (untreated, 10nM, 100nM, 1uM, 2uM, 5uM, 10uM, 20uM). The scale bars represent 75um.

Inhibition of the signature miRNA by Antagomir treatment was used to investigate its downstream effect. Fluorescent imaging shows transfection of the antagomir into the spheroids (figure 6). As expected, with a higher concentration of 1uM there was more antagomir transfected into the spheroids compared to a concentration of 100nM.

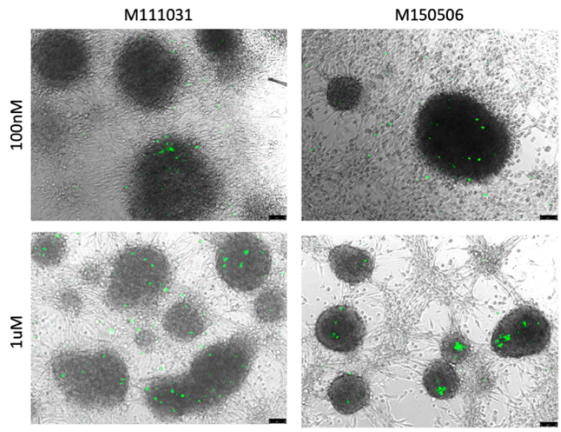

Figure 6. Antagomir transfection efficiency. Microscopic images overlay of fluorescent and bright field (10X magnification). Green fluorescence indicates 6FAM labeled antagomir 24h post treatment for different conditions (100nM and 1uM). Bright field images show the spheroids at day 4 of the two different BRAF cell lines (M111031 left; M150506 right). Scale bar represents 75um.

The BRAF signature miRNA hsa-mir-6728-3p is expressed in the EVs of cell lines M111031 and M150506 as shown by the sequencing data. M150536 was included as a control cell line, in which it was expected that the antagomir would not elicit any effect. Spheroids were formed and treated with 100nM of an antagomir for hsa-mir-6728-3p or negative control antagomir on day 2 and with 10uM of Vemurafenib on day 3. Cell viability was assessed on day 6 and plotted as percentage of untreated control (figure 7a) for the different conditions for each cell line. Representative bright field images of the spheroids for the three cell lines on day 6 for the different conditions are shown in figure 7b. No significant changes in viability were observed in conditions with antagomir compared to conditions without antagomir treatment for all cell lines. The experiment was repeated with the M150506 cell line, since this cell line had the highest expression of hsa-mir-6728-3p based on the sequencing data. In addition to 100nM, spheroids were also treated with 700nM, also in combination with Vemurafenib. Again, no changes were observed in cell viability compared to the untreated and negative control (supplementary figure 3).

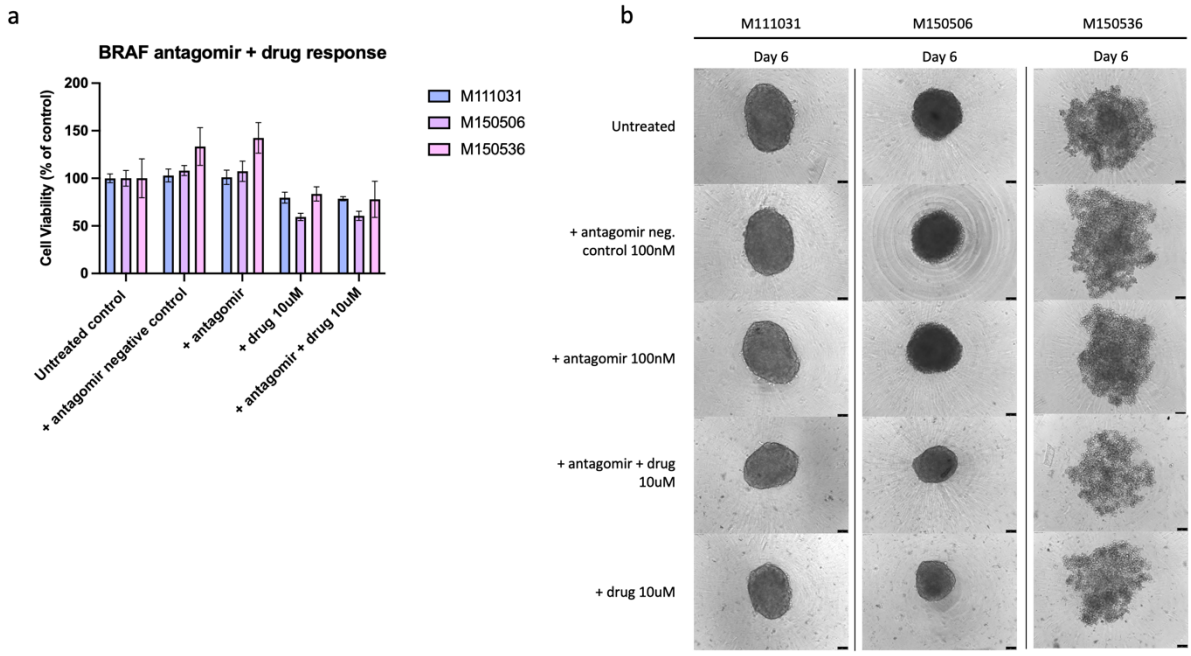

(legend on next page)

Figure 7. hsa-mir-6728-3p antagomir treatment does not affect cell viability and drug resistance. a) The effect of antagomir treatment for hsa-mir-6728-3p on Vemurafenib drug resistance and cell viability of BRAF spheroids (M111031=blue; M150506=purple; M150536=pink). Cell viability is expressed as percentage of control. Spheroids were treated with either a negative control antagomir or antagomir for hsa-mir-6728-3p with or without 10uM Vemurafenib. SD is indicated by the error bars; n=4. b) Representative bright field images (10X) for all cell lines and conditions at day 6. Scale bar represents 75um.

Silencing of hsa-mir-6728-3p reduces ITCH, Smurf2, and p-Smad2/3 expression

To validate if hsa-mir-6728-3p regulates the TGF-beta pathway, western blotting was performed. The two cell lines expressing hsa-mir-6728-3p in their EVs were treated with an antagomir for this miRNA in a 3D setting. Spheroids were treated with either an antagomir or a negative control antagomir with either 100nM or 1uM. GAPDH was used as housekeeping control. In addition, blots were stained for TGFBR1 and p-Smad2/3, important components of the TGF-beta pathway. Also, ITCH and SMURF2 were stained, since these proteins were predicted as targets of hsa-mir-6728-3p. Images of the blots and the quantified graphs are shown in figure 8. Conditions are normalized against the housekeeping control and the corresponding negative control was used to plot relative protein expression. Antagomir treatment reduced the relative protein expression of both ITCH and Smurf2 (figure 8a,b,c,d). For cell line M111031, ITCH inhibition was stronger in the 1uM dose compared to the 100nM dose, suggesting a dose-dependent effect. This dose response was not observed for ITCH in the cell line M150506. For Smurf2, a dose-dependent effect can be seen in cell line M150506, where a concentration of 1uM led to a stronger reduction in relative Smurf2 expression compared to 100nM of the antagomir. This dose-dependent effect was not observed for Smurf2 in the cell line M111031. Antagomir treatment also induced a reduction of p-Smad2/3 (figure 8e,f). This reduction was largest in M111031 and somewhat dose-dependent. The effect of antagomir treatment on TGFBR1 protein expression was less consistent. For M111031, TGFBR1 showed a reduction for the 1uM antagomir treatment condition. In contrast, M150506 showed a large increase in TGFBR1 for this condition (figure 8g,h).

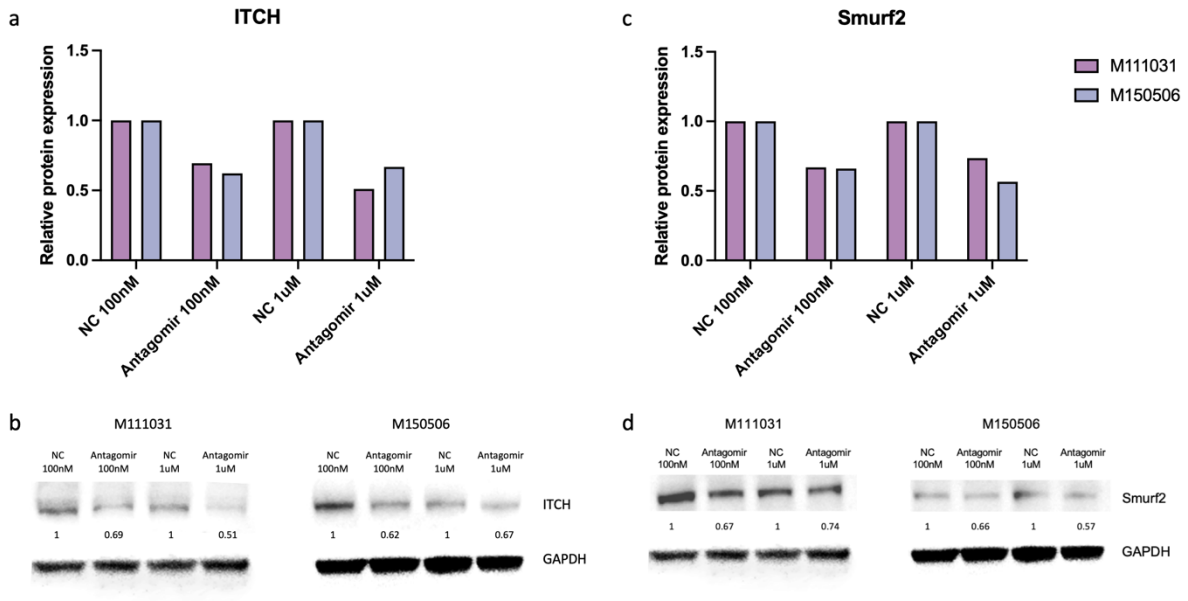

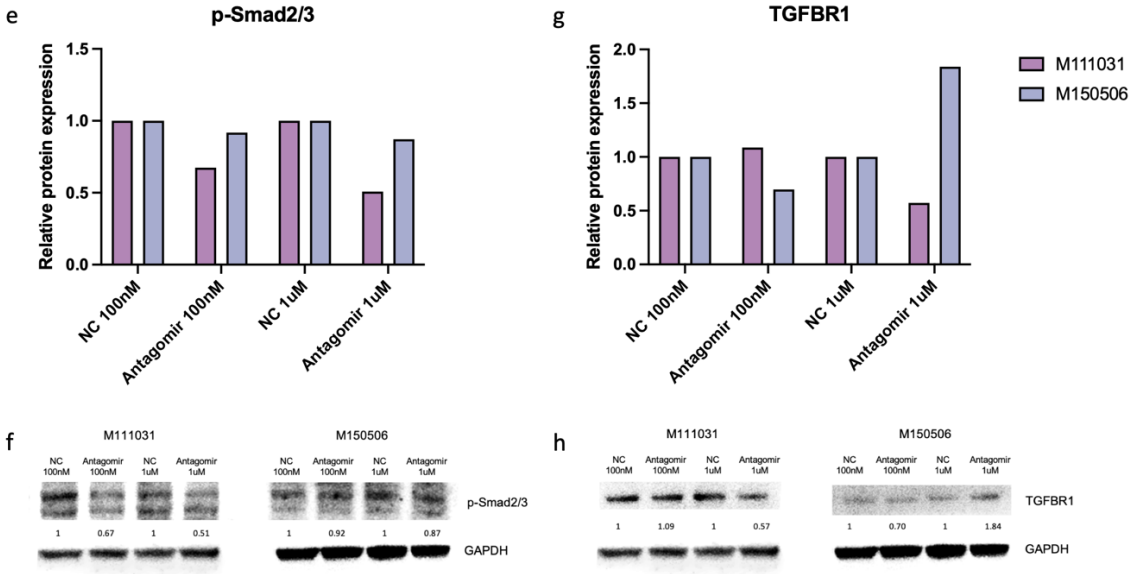

Figure 8. hsa-mir-6728-3p antagomir reduces ITCH, Smurf2, and p-Smad2/3 expression. a) Quantified graph showing the relative protein expression of ITCH with antagomir treatment compared to the negative control in two BRAF cell lines (M111031 and M150506). Protein expression values are plotted as relative to the negative control for both 100nM and 1uM antagomir treatment. Values are normalized against housekeeping control GAPDH. No replicates were performed. b) Western blot analysis of ITCH protein expression in M111031 and M150506 with antagomir or negative control antagomir treatment (100nm and 1uM). Normalized relative protein expression values are indicated. ITCH molecular weight is 113kDa. GAPDH molecular weight is 36kDa. c) Quantified graph showing the relative protein expression of Smurf2 with antagomir treatment compared to the negative control in two BRAF cell lines (M111031 and M150506). Protein expression values are plotted as relative to the negative control for both 100nM and 1uM antagomir treatment. Values are normalized against housekeeping control GAPDH. No replicates were performed. d) Western blot analysis of Smurf2 protein expression in M111031 and M150506 with antagomir or negative control antagomir treatment (100nm and 1uM). Normalized relative protein expression values are indicated. Smurf2 molecular weight is 80kDa. GAPDH molecular weight is 36kDa. e) Quantified graph showing the relative protein expression of p-Smad2/3 with antagomir treatment compared to the negative control in two BRAF cell lines (M111031 and M150506). Protein expression values are plotted as relative to the negative control for both 100nM and 1uM antagomir treatment. Values are normalized against housekeeping control GAPDH. No replicates were performed. f) Western blot analysis of p-Smad2/3 protein expression in M111031 and M150506 with antagomir or negative control antagomir treatment (100nm and 1uM). Normalized relative protein expression values are indicated. p-Smad2/3 molecular weight is 52/60kDa. GAPDH molecular weight is 36kDa. g) Quantified graph showing the relative protein expression of TGFBR1 with antagomir treatment compared to the negative control in two BRAF cell lines (M111031 and M150506). Protein expression values are plotted as relative to the negative control for both 100nM and 1uM antagomir treatment. Values are normalized against housekeeping control GAPDH. No replicates were performed. h) Western blot analysis of TGFBR1 protein expression in M111031 and M150506 with antagomir or negative control antagomir treatment (100nm and 1uM). Normalized relative protein expression values are indicated. TGFBR1 molecular weight is 56kDa. GAPDH molecular weight is 36kDa.

Silencing of hsa-mir-6836-3p does not affect the MAPK pathway

For the double mutant cell lines M121224 and M140906, hsa-mir-6836-3p was identified as candidate signature miRNA. It was hypothesized that if this miRNA is specifically sorted into EVs of these double mutant cell lines, it must play an important role in the tumorigenesis. Therefore, it was hypothesized that this candidate miRNA might regulate the MAPK pathway, crucial for the melanoma cancer phenotype. First, the IC50 curve for the double mutant cell lines was determined for both Vemurafenib and Binimetinib (figure 9). Spheroids were treated on day 3 with increasing concentrations of the drug (1uM, 2uM, 5uM, 10uM, and 20uM). Viability of the spheroids at day 5 after 48 hours of drug treatment is shown. The number of technical replicates is indicated with an n. Both M140906 and M121224 form dense spheroids. Binimetinib was much more potent in killing the cells than Vemurafenib. The largest reduction in cell viability with Binimetinib treatment occurs with a dose of 1uM. M140906 decreases in viability to 62% with 1uM compared to the untreated control. M121224 decreases in viability to 21% with 1uM compared to the untreated control. Vemurafenib treatment induces the largest

reduction in cell viability with a dose of 10uM. M140906 decreases in viability from 86% at 10uM to 61% at 20uM. M121224 decreases in viability from 69% at 10uM to 25% at 20uM. For subsequent experiments with double mutant cell lines, Vemurafenib was used with a dose of 10uM to study the effect of hsa-mir-6836-3p on the MAPK pathway and drug resistance.

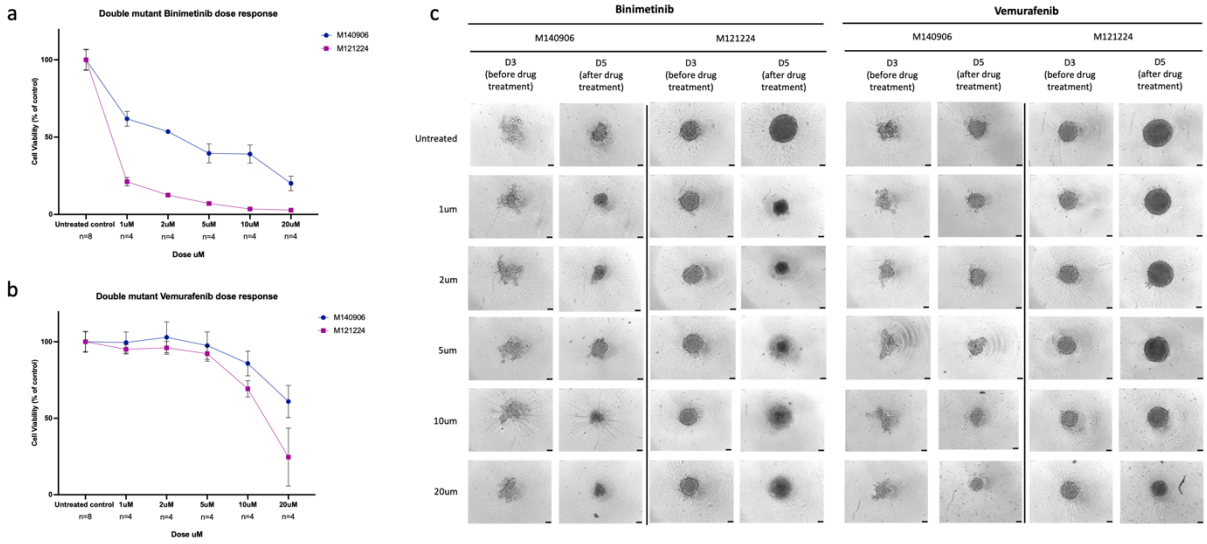

Figure 9. Vemurafenib and Binimetinib dose response in double mutant cell lines. a) Dose response of M140906 and M121224 to Binimetinib. For different doses of Binimetinib (untreated, 1uM, 2uM, 5uM, 10uM, 20uM), cell viability as percentage of control is plotted for the two double mutant cell lines (M140906=blue; M121224=pink). n = number of replicates. SD is indicated by the error bars. b) Dose response of M140906 and M121224 to Vemurafenib. For different doses of Vemurafenib (untreated, 1uM, 2uM, 5uM, 10uM, 20uM), cell viability as percentage of control is plotted for the two double mutant cell lines (M140906=blue; M121224=pink). n = number of replicates. SD is indicated by the error bars. c) Representative images (10X magnification) of spheroids from M140906 and M121224 on day 3 before drug treatment and on day 5 after 48h of drug treatment for different doses of Binimetinib and Vemurafenib (untreated, 1uM, 2uM, 5uM, 10uM, 20uM). Scale bar represents 75um.

Next, to investigate a possible regulatory role of candidate miRNA hsa-mir-3863-3p in the MAPK pathway, spheroids were treated with 100nM antagomir with or without 10uM Vemurafenib. Antagomir treatment did not affect morphology (supplementary figure 4). Western blot analysis was performed for RAF1, BRAF, and p-ERK1/2 (figure 10). Protein expression levels were normalized against the GAPDH housekeeping control. No differences in relative protein expression compared to the negative control were observed. As expected, the conditions treated with the BRAFV600E inhibitor Vemurafenib show a decrease in protein band intensity for p-ERK1/2 (figure 10f). By inhibiting the BRAF mutant, downstream pathway activation via the phosphorylation of ERK1/2 is reduced in both double mutant lines for this condition. However, antagomir treatment did not affect this drug response.

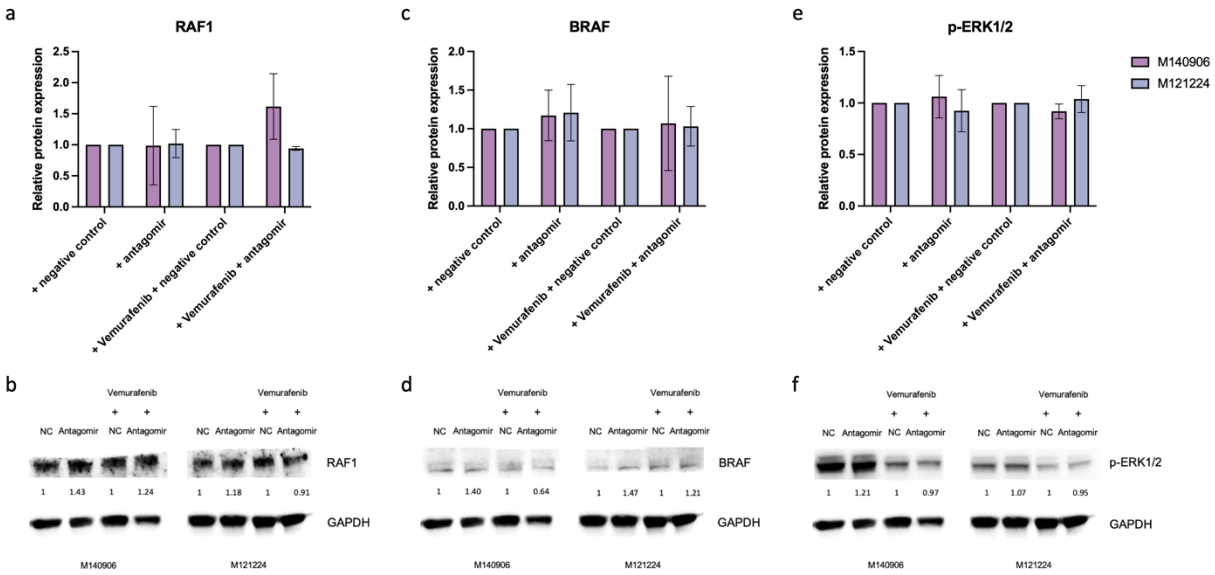

Figure 10. hsa-mir-6836-3p does not affect the MAPK pathway. a) Bar graph showing the western blot quantification of the effect of antagomir and drug treatment on RAF1 expression for double mutant cell lines M140906 and M121224. Data is shown as relative protein expression normalized against the housekeeping control GAPDH. Antagomir treatment was performed with a concentration of 100nM and drug treatment with a concentration of 10uM. SD is indicated by the error bars; n=2. b) Representative western blot images for RAF1 and housekeeping GAPDH for the different conditions (negative control, antagomir, negative control + Vemurafenib, antagomir + Vemurafenib). Relative expression values are shown as part of negative control. RAF1 molecular weight is 73kDa. GAPDH molecular weight is 36kDa. c) Bar graph showing the western blot quantification of the effect of antagomir and drug treatment on BRAF expression for double mutant cell lines M140906 and M121224. Data is shown as relative protein expression normalized against the housekeeping control GAPDH. Antagomir treatment was performed with a concentration of 100nM and drug treatment with a concentration of 10uM. SD is indicated by the error bars; n=2. d) Representative western blot images for BRAF and housekeeping GAPDH for the different conditions (negative control, antagomir, negative control + Vemurafenib, antagomir + Vemurafenib). Relative expression values are shown as part of negative control. BRAF molecular weight is 84kDa. GAPDH molecular weight is 36kDa. e) Bar graph showing the western blot quantification of the effect of antagomir and drug treatment on p-ERK1/2 expression for double mutant cell lines M140906 and M121224. Data is shown as relative protein expression normalized against the housekeeping control GAPDH. Antagomir treatment was performed with a concentration of 100nM and drug treatment with a concentration of 10uM. SD is indicated by the error bars; n=2. f) Representative western blot images for p-ERK1/2 and housekeeping GAPDH for the different conditions (negative control, antagomir, negative control + Vemurafenib, antagomir + Vemurafenib). Relative expression values are shown as part of negative control. p-ERK1/2 molecular weight is 38/43kDa. GAPDH molecular weight is 36kDa.

Cell type specific miRNA profiles

The next part of the report focusses on the in-silico analysis of the miRNA profiles. For each cell line the miRNA expression data from EV and cells was divided into three groups for subsequent bioinformatic analysis as explained above. Cell lines with less than 5 EV-enriched miRNAs or cell-retained miRNAs were excluded from the analysis, resulting in an EV vs cell miRNA enrichment data set for three BRAF, three NRAS, and four double mutant cell lines. The number of miRNAs in each group for all the cell lines and their corresponding mutation are shown in figure 11a. Selective distribution is calculated as the sum of EV-enriched and cell-retained miRNAs divided by the total number of miRNAs. For all lines, ~30% of the miRNAs display selective distribution in either cells or their corresponding EVs, meaning those miRNAs are either EV-enriched or cell-retained. EV-enriched miRNAs were compared between cell lines from the same mutant. Since neither BRAF, NRAS, or double mutant cell lines expressed miRNAs that were shared between all cell lines from the same mutant in EVs (supplementary figure 1), miRNAs were compared between all mutants that were expressed in at least two cell lines from the same mutant (figure 11b). This was repeated for the cell-retained miRNAs. The Venn diagram shows that for both EV-enriched and cell-retained miRNAs there is only one miRNA which is expressed in at least two cell lines from each mutant. This very limited overlap in miRNA expression between cell lines, even from the same mutant, and in both cell and EV

miRNA, underlines the existence of precisely regulated mechanisms for miRNA expression and sorting. There is no specific miRNA signature that all cell lines share in either cells or their EVs and therefore there does not seem to be a general melanoma-specific miRNA expression profile. However, as shown before, regarding mutant-specific miRNA expression, there are a number of miRNAs that are expressed in at least two of the cell lines for the BRAF and double mutants (supplementary figure 1).

To elucidate potential miRNA sorting mechanisms, the sequences from EV-enriched miRNAs and cell-retained miRNAs were analyzed. There was no general enrichment of 3p vs 5p miRNAs when comparing EVs and cells. It was previously reported that miRNAs that are sorted in EVs have a higher CG nucleotide content compared to the miRNAs retained in cells (22). CG content of the EV-enriched miRNAs and cell-retained miRNAs were compared for this melanoma dataset. In line with wat has previously been reported, EV-enriched miRNAs sequences had a significantly higher percentage of CG nucleotides compared to the cell-retained miRNA sequences (Figure10c, $p<0.05$).

a

Cell line	Mutation	Number of miRNAs			Total	Selective distribution
		Cell-retained Count≥3	Not enriched	EV-enriched Count≥2/FE≥3		
M111031	BRAF	34	99	7	140	29.3%
M150506	BRAF	29	108	10	147	26.5%
M150536	BRAF	31	100	13	144	30.6%
M140906	Double mutant	57	130	10	197	34.0%
M121224	Double mutant	28	99	21	148	33.1%
M150423	Double mutant	38	83	11	132	37.1%
M170917	Double mutant	16	67	11	94	28.7%
M130227	NRAS	16	64	12	92	30.4%
M131205	NRAS	5	72	33	110	34.5%
M130219	NRAS	13	54	17	84	35.7%

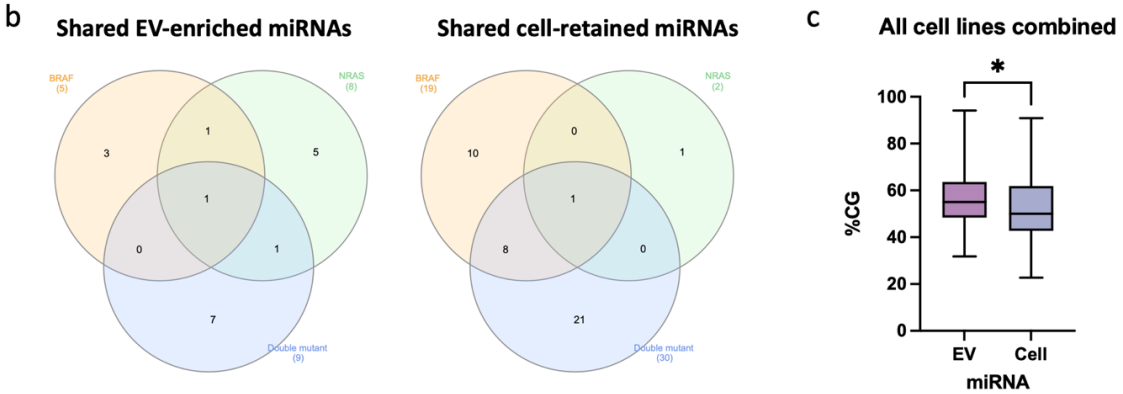

Figure 11. Selective distribution of miRNAs in EVs vs cells. a) Table showing the miRNA sequencing data set values for each cell line. For each cell line, mutation, number of cell-retained/EV-enriched/not-enriched/total miRNAs, and selective enrichment are shown. b) Venn-diagram showing the overlap in miRNAs between the three different mutants enriched in EVs (left) and retained in cells (right). miRNAs for each mutant were included if they were expressed in at least two cell lines of this mutant. For EV-enriched miRNAs, there is only one miRNA that at least two cell lines of each mutant share. Similarly, for cell retained miRNAs the different mutants only share one miRNA that is expressed in at least two cell lines of each mutant. c) Box-and-whiskers-plot showing the percentage of CG nucleotides in the sequences of EV-enriched vs cell-retained miRNAs. Min and max values are indicated by the whiskers. The median is indicated by the line in the middle of the box. EV-enriched miRNA (mean = 56.22) had a significantly higher percentage of CG nucleotides compared to cell-retained miRNA (mean = 52.69) ($p<0.05$). Significance was determined by unpaired t-testing.

Role of miRNA sequence in miRNA sorting

Building on a previously proposed mechanism for miRNA sorting via 'motif-sequences' within the miRNA sequences, in silico motif enrichment analysis was performed as explained in the methods section. For each cell line, the identified motifs for both EV-enriched miRNA (EXO motifs) and cell-retained miRNA (CELL motifs) are shown in figure 12. The analysis tool establishes a relatively enriched motif from the input sequences compared to the control sequences, indicating the relative contribution of each nucleotide to the motif. The motif enrichment analysis tends to favor longer motif sequences. However, the input sequences contributing to the motif do not necessarily need to have the exact motif in their sequence, but rather only partly contribute to the motif with only a few nucleotides. Therefore, in the extended motifs, gaps may occur for which there is no relative enrichment of a certain nucleotide in the sequences contributing to the motifs, or more than one nucleotide is relatively enriched for that position. This results in low occurrence of these 'extended' motifs in the miRNA sequences dataset. From the extended motifs, we therefore identified a short 4-nucleotide core motif, with the highest occurrence in the input miRNA sequences. For each cell line 1 to 5 EXO motifs and 1 to 5 CELL motifs of 4-7 nucleotides could be identified, with the exception of cell line M130227 for which no CELL motifs could be identified. Only motifs for which the extended motif had a 0% occurrence in the control sequences and an E-value of <0.005 and the core motifs had at least 20% occurrence in the input sequences and a FE of >3 were included. Core EXO motifs had on average 63.3% CG content compared to 45.5% CG content in CELL motifs. The core EXO motifs could be found in 20.0%-50.0% of the miRNA sequences. The core CELL motifs could be found in 20.0% to 43.8% of the miRNA sequences. Interestingly, more EV motifs meeting the inclusion criteria could be identified than cell motifs.

In addition to the high cell line specificity of miRNAs, the majority of enriched motifs are also cell line specific. However, some motifs are found in multiple cell lines. For example, C/GUCC is shared between all BRAF mutant cell lines. Also, CCGG is shared between two double mutant cell lines, and GGGA and CGUG is shared between Double mutant and NRAS cell lines. There does not seem to be an additive effect of the motifs, meaning the miRNAs with the highest read counts do not necessarily have more motifs in their sequence. Interestingly, both EV and CELL motifs primarily occur in the 3' end of the miRNA sequences (figure 13). The bar graphs show the position of the motifs grouped in either the first half (5') defined as nucleotide 1-9 or second half (3') defined as nucleotide 10 - 3'end. The seed region of miRNAs is located at the 5' end of the sequence, while the identified motifs thus seem to be located away from this seed region at the 3' end of the sequence.

a

	Extended EXO motifs				Core EXO motifs			
	Motif	E-value extended motif	% EV miRNAs	% cell miRNAs	Motif	% EV miRNAs	% cell miRNAs	Fold enrichment
M111031		3.1e-005	85.7%	0.0%	CUCC	28.6%	6.25%	4.6
		5.6e-003	42.9%	0.0%	CCCC	42.9%	0%	n/a
		3.2e-002	28.6%	0.0%	CGGG	28.6%	2.3%	18.7
M150506		2.9e-004	60.0%	0.0%	CUCC	40.0%	6.9%	5.8
		2.9e-004	60.0%	0.0%	CCCA	50.0%	10.3%	4.9
		4.3e-003	40.0%	0.0%	CUGC	30.0%	6.9%	4.3
		1.7e-002	30.0%	0.0%	UUCU	30.0%	0.0%	n/a
		1.7e-002	30.0%	0.0%	GCUC	30.0%	3.4%	8.8
M150536		7.2e-003	30.8%	0.0%	UCUC	30.8%	9.7%	3.2
		2.5e-002	23.1%	0.0%	CUGA	23.1%	3.2%	7.2
		7.2e-003	30.8%	0.0%	UCUG	30.8%	6.5%	4.7
		6.0e-004	46.2%	0.0%	GUCC	23.1%	0.0%	n/a
		2.4e-002	23.1%	0.0%	GCAC	23.1%	6.5%	3.6

b

	Extended CELL motifs				Core CELL motifs			
	Motif	E-value extended motif	% EV miRNAs	% cell miRNAs	Motif	% EV miRNAs	% cell miRNAs	Fold enrichment
M111031		5.1e-003	84.4%	0.0%	UGCA	20.6%	0.0%	n/a
		3.6e-002	53.1%	0.0%	UAGG	23.5%	0.0%	n/a
M150506		2.5e-004	96.6%	0.0%	GUUG	27.6%	0.0%	n/a
M150536		4.5e-002	29.0%	0.0%	CUUU	29.0%	7.7%	3.8
		1.1e-003	64.5%	0.0%	CAA	22.6%	0.0%	n/a

	Extended EXO motifs				Core EXO motifs			
	Motif	E-value extended motif	% EV miRNAs	% cell miRNAs	Motif	% EV miRNAs	% cell miRNAs	Fold enrichment
M140906		4.7e-004	40.0%	0.0%	GAGU	20.0%	0.0%	n/a
		3.2e-003	30.0%	0.0%	CCGG	30.0%	0.0%	n/a
M121224		3.4e-002	19.0%	0.0%	CCGG	23.8%	3.4%	7
M150423		6.2e-004	45.5%	0.0%	GUAC	27.3%	2.6%	10.5
		2.7e-003	36.4%	0.0%	AUCU	27.3%	2.6%	10.5
M170917		2.8e-002	36.4%	0.0%	GCUG	36.4%	6.3%	5.8
		2.8e-002	36.4%	0.0%	GGGA	27.3%	0.0%	n/a

	Extended CELL motifs				Core CELL motifs			
	Motif	E-value extended motif	% EV miRNAs	% cell miRNAs	Motif	% EV miRNAs	% cell miRNAs	Fold enrichment
M140906		7.7e-004	78.9%	0.0%	GUAG	22.8%	0.0%	n/a
M121224		2.3e-002	25%	0.0%	GGUU	20.7%	4.8%	4.3
M150423		4.9e-004	81.6%	0.0%	UGUG	26.3%	0.0%	n/a
		3.5e-003	60.5%	0.0%	CUCU	21.1%	0.0%	n/a
M170917		6.7e-003	62.5%	0.0%	GAC	43.8%	9.1%	4.8

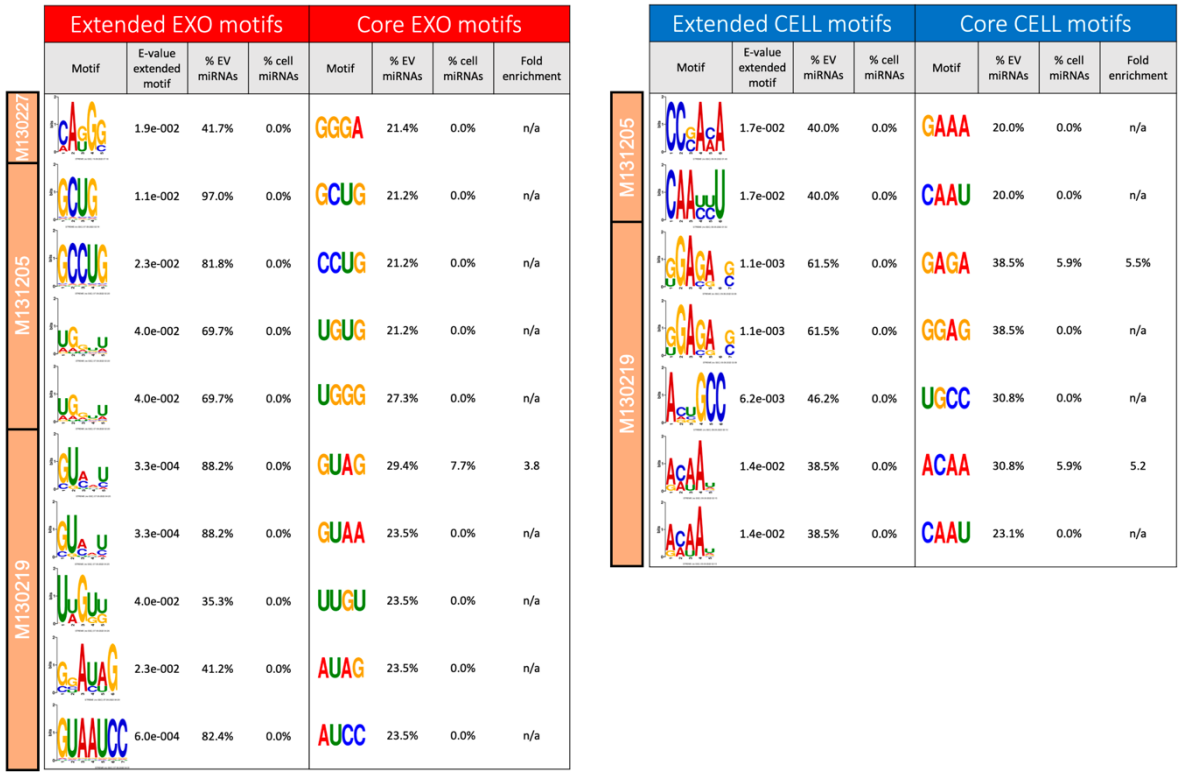

	Extended EXO motifs				Core EXO motifs			
	Motif	E-value extended motif	% EV miRNAs	% cell miRNAs	Motif	% EV miRNAs	% cell miRNAs	Fold enrichment
M130227		1.9e-002	41.7%	0.0%	GGGA	21.4%	0.0%	n/a
M131205		1.1e-002	97.0%	0.0%	GCUG	21.2%	0.0%	n/a
		2.3e-002	81.8%	0.0%	CCUG	21.2%	0.0%	n/a
		4.0e-002	69.7%	0.0%	UGUG	21.2%	0.0%	n/a
		4.0e-002	69.7%	0.0%	UGGG	27.3%	0.0%	n/a
M130219		3.3e-004	88.2%	0.0%	GUAG	29.4%	7.7%	3.8
		3.3e-004	88.2%	0.0%	GUAA	23.5%	0.0%	n/a
		4.0e-002	35.3%	0.0%	UUGU	23.5%	0.0%	n/a
		2.3e-002	41.2%	0.0%	AUAG	23.5%	0.0%	n/a
		6.0e-004	82.4%	0.0%	AUCC	23.5%	0.0%	n/a

	Extended CELL motifs				Core CELL motifs			
	Motif	E-value extended motif	% EV miRNAs	% cell miRNAs	Motif	% EV miRNAs	% cell miRNAs	Fold enrichment
M131205		1.7e-002	40.0%	0.0%	GAAA	20.0%	0.0%	n/a
		1.7e-002	40.0%	0.0%	CAAU	20.0%	0.0%	n/a
M130219		1.1e-003	61.5%	0.0%	GAGA	38.5%	5.9%	5.5%
		1.1e-003	61.5%	0.0%	GGAG	38.5%	0.0%	n/a
		6.2e-003	46.2%	0.0%	UGCC	30.8%	0.0%	n/a
		1.4e-002	38.5%	0.0%	ACAA	30.8%	5.9%	5.2
		1.4e-002	38.5%	0.0%	CAAU	23.1%	0.0%	n/a

Figure 12. Motifs enriched in miRNAs preferentially sorted into EVs or retained in cells for each cell line. a) Table showing the Extended (left) and Core (right) sequence motifs identified for miRNAs enriched in EVs (EXO motifs; Red). Cell line is indicated on the right and mutation is indicated by color (Green = BRAF; Yellow = double mutant; Orange = NRAS). For each extended motif, E-value, percentage of input miRNAs containing the motif, and percentage of control miRNAs containing the motif are indicated. For each associated CORE motif, percentage of input and control miRNA sequences containing the motif and the fold enrichment (ratio between previous two columns) are indicated. b) Table showing the Extended (left) and Core (right) sequence motifs identified for miRNAs retained in cells (CELL motifs; Blue). Cell line is indicated on the right and mutation is indicated by color (Green = BRAF; Yellow = double mutant; Orange = NRAS). Values shown are similar as in a.

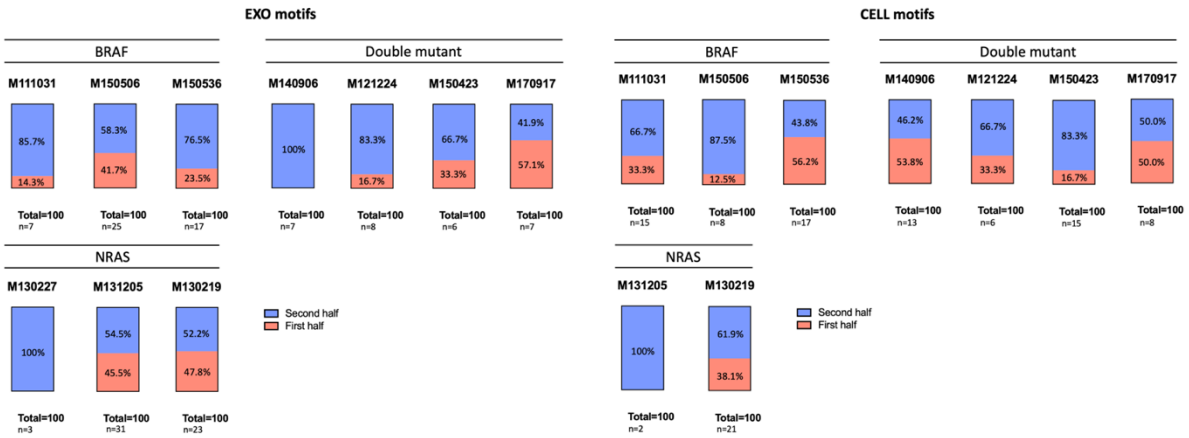

Figure 13. Position of over-represented motifs in miRNA sequences of EV-enriched and cell-retained miRNAs. Left, bar graphs showing the position distribution of the core EXO motifs identified for each cell line in either the first half (orange; nucleotide 1-9) or second half (purple; nucleotide 10 - 3'end) of the miRNA sequence. Distribution of all enriched EXO motifs are combined for each cell line (Total percentage of miRNAs = 100). Right, bar graphs showing the position distribution of the core CELL motifs identified for each cell line in either the first half (orange; nucleotide 1-9) or second half (purple; nucleotide 10 - 3'end) of the miRNA sequence. Distribution of all enriched CELL motifs are combined for each cell line (Total percentage of miRNAs = 100).

Discussion

Malignant cells alter the secretion of EVs and their cargo (27,28). Accumulating evidence suggest a biologically active role of EVs in health and disease. However, the exact mechanisms by which oncogenic signaling affects EV cargo composition remain elusive. Since secreted miRNAs in EVs are capable of modulating the TME, it is of great relevance to understand the pathways of selective cargo sorting into EVs. It was recently demonstrated that in the plasma of melanoma patients, melanoma-derived EVs can be detected, comprising 23-66% of the total EVs (29). This offers an opportunity to develop EV-based diagnostic methods for melanoma, since EVs contain information about their cell of origin. In support of this hypothesis, a similar study of EV-miRNA in colorectal cancer with wild type or mutant KRAS status already showed a mutant-dependent miRNA expression profile in EVs (30). Currently, melanoma-specific miRNA profiles in secreted EVs have not yet been established. In this report, we comprehensively examined the miRNA profiles from EVs and cells of patient-derived melanoma cell lines differing in mutation (BRAF, NRAS, double mutant). We showed that miRNA sorting into EVs differs per cell line and miRNA enrichment in EVs is clearly distinct from the miRNA profile present in the cell of origin, even with cell lines of similar genetic background. These observations suggest that mechanisms for selective cargo sorting exist, adapted to the specific need of cells. We identified BRAF and double mutant specific miRNAs. Mutant status-dependent miRNA sorting supports the idea of using EVs in melanoma diagnosis as potential biomarkers.

The functional role of miRNAs secreted in cancer-derived EVs in promoting tumorigenesis remains largely unknown. For hsa-mir-6728-3p and hsa-mir-6836-3p it is unclear whether the expression and secretion of these signature miRNAs are associated with oncogenic signaling. Since they are mutant-dependent, it is likely that these miRNAs are involved in tumorigenesis. Based on our western blot data, hsa-mir-6728-3p in vitro enhances TGF-beta signaling by the phosphorylation of Smad2/3, possibly via its regulation by ITCH. Interestingly, we hypothesized antagomir silencing would increase the expression of the miRNA targets, because of its inhibitory role. However, expression of ITCH and Smurf2 was reduced with antagomir treatment. ITCH and Smurf2 are both E3 ligases that can ubiquitinate many substrates (31-34). Previous studies have shown that their expression is regulated via auto-inhibition. In an inactive state, both ITCH and Smurf2 undergo a conformational change and bind to itself (35,36). It can be hypothesized that the miRNA hsa-mir-6728-3p can bind to these proteins thereby preventing the autoinhibition.

The TGF-beta pathway has been well-studied in the context of melanoma and tumorigenesis in general. It has been frequently observed to be increased in melanoma and is known to alter immune surveillance, drug resistance and the TME (37,38). However, mechanisms behind this increase in TGF-beta signaling remained elusive. Our data, suggests hsa-mir-6728-3p as a possible regulator capable of enhancing signaling via this pathway. This supports an active functional role of EV-miRNAs secreted by cancer cells in disease progression. Target prediction can be a useful tool to identify and subsequently validate targets for miRNAs. However, additional validation is necessary to further prove the role of hsa-mir-6728-3p in TGF-beta signaling regulation since experiments were only performed once and changes were only observed in one of the two BRAF cell lines known that express this miRNA.

Our finding that mutant-specific miRNA profiles exist and that these signature miRNAs can regulate important pathways such as TGF- beta in vitro raises interesting questions regarding how they are selected for preferential sorting. Analysis of the miRNA sequences identified EV-

export (EXO motifs) and cell-retention (CELL motifs) motifs. While the evidence is clear that miRNAs in EVs can modify the cellular microenvironment and miRNA sorting into EVs is altered in disease, how these specific miRNAs are packaged into EVs remains mostly unknown. Previous studies have reported EV sequence motifs and RNA-binding proteins, such as Alyref, Fus, and SYNCRIP, correlated with their localization into EVs (22-25). In contrast, non-selective mechanisms of miRNA sorting have also been described (21,39). Our data suggest it is an integrated and complex mechanism potentially involving both non-selective and selective sorting mechanisms depending on multiple sequence motifs and RNA-binding proteins with high cell-type specificity. The enrichment of certain miRNAs in EVs or retention in cells with fold changes of more than 100 and 400 respectively underlines the presence of selective sorting mechanisms. On the other hand, a substantial number of miRNAs show no selective enrichment in either cells or EVs, suggesting non-selective sorting occurs in parallel with selective sorting. The identified EXO sequence motifs in our data, differ between cell lines, even cell lines with the same mutation. However, similarities can be seen as highlighted before. Cancer cells are known to secrete more EVs than their healthy counterparts and alter their miRNA profiles (26). It is, however, largely unknown which of the miRNAs in the expression profile from our cell lines contribute to tumorigeneses and which miRNA expression is involved in normal homeostasis mechanisms, since validated targets have not been reported. It can be hypothesized that the miRNAs contributing to normal cell-to-cell signaling or homeostasis are conserved across different cell types and perhaps even species. The identified over-represented motifs that are shared between miRNAs of different cell lines could therefore be more conserved and thus attributed to normal cell signaling instead of tumorigenesis.

The cell type specific or mutant specific motif sequences could underline altered miRNA sorting in tumor cells. Comparing the motifs identified in our dataset to previously identified motifs provides an additional layer of interpreting these motifs. A recent publication by Garcia-Martin et al. analyzed miRNA in cells and EVs of five different mouse cell lines (white adipocytes, brown adipocytes, endothelial cells, skeletal muscle cells, and hepatocytes). Interestingly, certain EXO motifs (UGUG, CGGG, CCUC) were also identified in our data set, indicating a conserved nature. In addition to the identical shared motifs, there was also a number of motifs almost identical to the ones identified in that study, for example, AGGG instead of GGGA and GGCC instead of CCGG. Regarding the CELL motifs, there was less similarity. Only GUAG. While the consensus on the existence of EV sorting motifs is strong, the existence of cell-retention motifs is less often reported (22). It can be hypothesized that for miRNAs to be retained in the cells it is only required that the sequence does not contain EV sorting motifs or the cell does not have the machinery to recognize sequence motifs in those miRNAs to export them out. The sequence motifs identified in this study cannot fully explain the sorting of all the EV-enriched or cell-retained miRNAs, since some of the EV-enriched or cell-retained miRNA sequences do not contain any of the identified motifs. One possibility is that the motif enrichment analysis simply could not identify all motifs because of the limited number of miRNAs and thus limited occurrence of motifs. Perhaps certain sequences that were not identified as motifs are in vivo still recognized by sorting proteins.

Selective enrichment of miRNAs in either EVs or their cell of origin is in the first place depends on the regulation of miRNA expression. Besides the fact that in order to be packaged in EVs, miRNAs need to be expressed in the cell, the cell also need to have the machinery that is able to recognize and sort specific miRNAs based on their EXO motif. In the proposed model for miRNA sorting (figure 2), certain RNA-interacting proteins can recognize the repertoire of EV and cell sequence motifs and promote their sorting accordingly. In addition to the differences in miRNAs and thus sequence motifs between cell lines, this machinery also differs. Only this

difference in sorting machinery could explain why some miRNAs in one cell type are retained in the cell while in the other cell type they are exported into EVs. For example, in our data, miRNA hsa-mir-6850-5p has a read count of 26 in EVs and 0 in cells of cell line M121224 while in M150423 it has a read count of 0 in EVs and 12 in cells. Looking at its sequence and the identified motifs for those cell lines, the M121224 EXO motif CCGG is present. None of the EXO motifs identified for M150423 are present in the sequence, supporting the relevance of these motifs. hsa-mir-6850-5p is retained in the cells of M150423, however, the sequence does not contain any of the identified CELL motifs for that cell line. This suggests that the lack of machinery to identify certain sequences is sufficient to retain miRNAs in cells, without the need for CELL motifs. Interestingly, the CELL motifs identified for M150423, UGUG and CUGU, are similar to EXO motifs identified in other cell lines. Instead of categorizing these motifs as cell motifs, another explanation is that this cell type simply does not have the machinery to recognize these sequence motifs, therefore the miRNAs with these motifs remain in the cells. Thus, since the mature miRNA sequences don't change between cells, but their expression and localization can change, this indicates that cells depend on different machinery to sort miRNAs into EVs and this can be characterized as a highly cell specific mechanism. It remains a big knowledge gap how a cell acquires this specific process and what determines how some cells can export certain miRNAs while other cell types can't.

This report shows how highly variable the miRNA expression profiles are, even from cell lines with the same genetic mutation. The signature miRNAs hsa-mir-6728-3p for BRAF cell lines and hsa-mir-6836-3p for the double mutant cell lines contain the EXO motifs in their sequence that are identified for the cell lines in which this miRNA was expressed. For M111031 and M150506, hsa-mir-6728-3p contains the sequence motifs CUCC, CCCC, CCCA, CUGC, UCUG. For M121224 and M140906, hsa-mir-6836-3p contains the sequence motif CCGG. The higher CG content in EV-enriched miRNA sequences translates to a higher CG content in the EXO motifs compared to the CELL motifs. Because of the short length of miRNA sequences, slight changes in nucleotide composition can drastically affect CG content of the sequence. It is believed CG content affects target binding and stability of the miRNA. But conclusive evidence is lacking. In addition, the localization of the identified motifs primarily at the 3'end of the miRNA sequences further supports the existence of motifs. The question why miRNAs with certain motifs are exported into EVs with higher read counts than others cannot be answered based on our data. The number of motifs in the sequence does not seem to be correlated to higher read counts in EVs. The answer might involve more efficient machinery for some motifs or merely the fact that some miRNAs are expressed in higher numbers and therefore higher in EVs.

An important next step to validate if these motifs are sufficient to control miRNA distribution between cells and EVs would be in vitro mutagenesis experiments. Previous researchers have shown that by mutating an EXO motif, miRNAs showed decreased sorting into EVs (22,24,25). In addition, introducing an EXO sequence to a cell-miRNA, resulted in increased sorting of this miRNA into EVs. By contrast, introducing a CELL motif to a miRNA enriched in EVs resulted in increased retention in cells. This could show the relevance of each single motif in EV sorting or cell retention of miRNAs in different cell lines. While our data further contributes to the concept of miRNA sorting as a complex and integrated cell type specific mechanism depending on miRNA expression and protein-sorting machinery, the full sorting system remains to be determined. Understanding this mechanism will not only help to better be able to identify the cells of origin of circulating miRNAs, but also provide possibilities to exploit this mechanism for therapeutic purposes.

In addition, the effectiveness of inhibiting the miRNA of interest with an antagomir has not been evaluated. Since the miRNA hsa-mir-6728-3p is only expressed in EVs, silencing might not be as straightforward as silencing of cell-retained miRNAs. If miRNAs that are selectively sorted into EVs can be inhibited by antagomirs intracellularly before there export into EVs is unknown. We hypothesize that this is the most likely mechanism, since antagomir silencing once the miRNA is located in an EV seems unlikely. Also, miRNA expression might change over time within the cell lines. Whether or not the candidate signature miRNA that was identified based on the sequencing data is still expressed in the EVs of these cell lines over a longer period of time was not determined. It might explain the difference in response between the two cell lines. Another important aspect of regulation by this miRNA selectively sorted in EVs, is that it is unknown whether the miRNA targets primarily the local TME and other melanoma cells or elicits a more distal effect in for example immune cells. Co-culture experiments with immune cells could further elucidate the role of this miRNA.

Once a miRNA target has been identified and validated in vitro, it would be interesting to compare the data with patient-samples to see if similar miRNAs are expressed. Important to note, the identification of miRNA targets is challenging and for many miRNAs their actual targets remain unknown. It is however commonly accepted that miRNAs are crucial regulators with far-reaching effects. Thus, unravelling these complex regulatory networks of miRNA signaling is of great importance to better understand cell-to-cell communication in health and disease. This could potentially contribute to improving diagnostics and the development of new therapeutic targets.

References

(1) Shain AH, Bastian BC. From melanocytes to melanomas. Nature Reviews Cancer 2016;16(6):345-358.

(2) Leonardi G,C., Falzone L, Salemi R, Zanghì A, Spandidos D,A., Mccubrey J,A., et al. Cutaneous melanoma: From pathogenesis to therapy (Review). Int J Oncol 2018;52(4):1071-1080.

(3) Bastian BC. The molecular pathology of melanoma: an integrated taxonomy of melanocytic neoplasia. Annu Rev Pathol 2014;9:239-271.

(4) Lugović-Mihić L, Ćesić D, Vuković P, Novak Bilić G, Šitum M, Špoljar S. Melanoma Development: Current Knowledge on Melanoma Pathogenesis. Acta Dermatovenerol Croat 2019 Sep;27(3):163-168.

(5) Delevoye C. Melanin Transfer: The Keratinocytes Are More than Gluttons. J Invest Dermatol 2014;134(4):877-879.

(6) Viros A, Sanchez-Laorden B, Pedersen M, Furney SJ, Rae J, Hogan K, et al. Ultraviolet radiation accelerates BRAF-driven melanomagenesis by targeting TP53. Nature 2014;511(7510):478-482.

(7) Sample A, He YY. Mechanisms and prevention of UV-induced melanoma. Photodermatol Photoimmunol Photomed 2018 Jan;34(1):13-24.

(8) Curtin JA, Fridlyand J, Kageshita T, Patel HN, Busam KJ, Kutzner H, et al. Distinct Sets of Genetic Alterations in Melanoma. N Engl J Med 2005;353(20):2135-2147.

(9) Guo W, Wang H, Li C. Signal pathways of melanoma and targeted therapy. Signal Transduction and Targeted Therapy 2021;6(1):424.

(10) Reddy BY, Miller DM, Tsao H. Somatic driver mutations in melanoma. Cancer 2017;123:2104-2117.

(11) Bertolotto C. Melanoma: from melanocyte to genetic alterations and clinical options. Scientifica (Cairo) 2013;2013:635203.

(12) Raaijmakers MI, Widmer DS, Narechania A, Eichhoff O, Freiberger SN, Wenzina J, et al. Co-existence of BRAF and NRAS driver mutations in the same melanoma cells results in heterogeneity of targeted therapy resistance. Oncotarget 2016 Nov 22;7(47):77163-77174.

(13) Curti BD, Faries MB. Recent Advances in the Treatment of Melanoma. N Engl J Med 2021;384(23):2229-2240.

(14) Moreira A, Heinzerling L, Bhardwaj N, Friedlander P. Current Melanoma Treatments: Where Do We Stand? Cancers 2021 Jan 9,;13(2):221.

(15) Weinstein D, Leininger J, Hamby C, Safai B. Diagnostic and prognostic biomarkers in melanoma. J Clin Aesthet Dermatol 2014 Jun;7(6):13-24.

(16) Reddy KB. MicroRNA (miRNA) in cancer. Cancer Cell International 2015;15(1):38.

(17) Balacescu O, Sur D, Cainap C, Visan S, Cruceriu D, Manzat-Saplacan R, et al. The Impact of miRNA in Colorectal Cancer Progression and Its Liver Metastases. International Journal of Molecular Sciences 2018;19(12).

(18) Kandettu A, Radhakrishnan R, Chakrabarty S, Sriharikrishnaa S, Kabekkodu SP. The emerging role of miRNA clusters in breast cancer progression. Biochimica et Biophysica Acta (BBA) - Reviews on Cancer 2020;1874(2):188413.

(19) Crescitelli R, Lässer C, Szabó TG, Kittel A, Eldh M, Dianzani I, et al. Distinct RNA profiles in subpopulations of extracellular vesicles: apoptotic bodies, microvesicles and exosomes. Journal of Extracellular Vesicles 2013;2(1):20677.

(20) Valadi H, Ekström K, Bossios A, Sjöstrand M, Lee JJ, Lötvall J,O. Exosome-mediated transfer of mRNAs and microRNAs is a novel mechanism of genetic exchange between cells. Nat Cell Biol 2007;9(6):654-659.

(21) Temoche-Diaz M, Shurtleff MJ, Nottingham RM, Yao J, Fadadu RP, Lambowitz AM, et al. Distinct mechanisms of microRNA sorting into cancer cell-derived extracellular vesicle subtypes. eLife 2019;8:e47544.

(22) Garcia-Martin R, Wang G, Brandão BB, Zanotto TM, Shah S, Kumar Patel S, et al. MicroRNA sequence codes for small extracellular vesicle release and cellular retention. Nature 2022;601(7893):446-451.

(23) Villarroya-Beltri C, Gutiérrez-Vázquez C, Sánchez-Cabo F, Pérez-Hernández D, Vázquez J, Martin-Cofreces N, et al. Sumoylated hnRNPA2B1 controls the sorting of miRNAs into exosomes through binding to specific motifs. Nature Communications 2013;4(1):2980.

(24) Shurtleff MJ, Temoche-Diaz M, Karfilis KV, Ri S, Schekman R. Y-box protein 1 is required to sort microRNAs into exosomes in cells and in a cell-free reaction. eLife 2016;5:e19276.

(25) Santangelo L, Giurato G, Cicchini C, Montaldo C, Mancone C, Tarallo R, et al. The RNA-Binding Protein SYNCRIP Is a Component of the Hepatocyte Exosomal Machinery Controlling MicroRNA Sorting. Cell Reports 2016;17(3):799-808.

(26) Vasconcelos MH, Caires HR, Ābols A, Xavier CPR, Linē A. Extracellular vesicles as a novel source of biomarkers in liquid biopsies for monitoring cancer progression and drug resistance. Drug Resistance Updates 2019;47:100647.

(27) Tucci M, Mannavola F, Passarelli A, Stucci LS, Cives M, Silvestris F. Exosomes in melanoma: a role in tumor progression, metastasis and impaired immune system activity. Oncotarget 2018 Apr 17;9(29):20826-20837.

(28) Melo SA, Sugimoto H, O'Connell JT, Kato N, Villanueva A, Vidal A, et al. Cancer Exosomes Perform Cell-Independent MicroRNA Biogenesis and Promote Tumorigenesis. Cancer Cell 2014;26(5):707-721.

(29) Sharma P, Diergaarde B, Ferrone S, Kirkwood JM, Whiteside TL. Melanoma cell-derived exosomes in plasma of melanoma patients suppress functions of immune effector cells. Scientific Reports 2020;10(1):92.

(30) Cha DJ, Franklin JL, Dou Y, Liu Q, Higginbotham JN, Demory Beckler M, et al. KRAS-dependent sorting of miRNA to exosomes. Elife 2015 Jul 1;4:e07197.

(31) Salah Z, Melino G, Aqeilan RI. Negative Regulation of the Hippo Pathway by E3 Ubiquitin Ligase ITCH Is Sufficient to Promote Tumorigenicity. Cancer Res 2011;71(5):2010-2020.

(32) Aki D, Zhang W, Liu Y. The E3 ligase Itch in immune regulation and beyond. Immunol Rev 2015;266(1):6-26.

(33) Yin Q, Wyatt CJ, Han T, Smalley KSM, Wan L. ITCH as a potential therapeutic target in human cancers. Semin Cancer Biol 2020;67:117-130.

(34) Fu L, Cui C, Zhang X, Zhang L. The functions and regulation of Smurfs in cancers. Semin Cancer Biol 2020;67:102-116.

(35) Scialpi F, Malatesta M, Peschiaroli A, Rossi M, Melino G, Bernassola F. Itch self-polyubiquitylation occurs through lysine-63 linkages. Biochem Pharmacol 2008;76(11):1515-1521.

(36) Wiesner S, Ogunjimi AA, Wang H, Rotin D, Sicheri F, Wrana JL, et al. Autoinhibition of the HECT-Type Ubiquitin Ligase Smurf2 through Its C2 Domain. Cell 2007;130(4):651-662.

(37) Busse A, Keilholz U. Role of TGF-β in melanoma. Curr Pharm Biotechnol 2011 Dec;12(12):2165-2175.

(38) Colak S, ten Dijke P. Targeting TGF-β Signaling in Cancer. Trends in Cancer 2017;3(1):56-71.

(39) Tosar JP, Gámbaro F, Sanguinetti J, Bonilla B, Witwer KW, Cayota A. Assessment of small RNA sorting into different extracellular fractions revealed by high-throughput sequencing of breast cell lines. Nucleic Acids Res 2015;43(11):5601-5616.

Supplementary data

Supplementary Table 1. Western blot buffers

Transfer buffer
- Glycine (7.2g)
- Tris base (1.51g)
- Methanol (50ml)
- ddH2O (up to 500ml)

10X TBST
- Tris base (24g)
- NaCl (88g)
- ddH2O up to 1L
- Adjust the pH to 7.6

TBST
- 1X TBS
- 1% Tween20

Mild-stripping buffer
- Glycine (7.5g)
- SDS (0.5)
- Tween 20 (5ml)
- ddH2O (up to 500ml)
- Adjust pH to 2.2

Supplementary Table 2. Primary and secondary antibodies

Primary antibodies	**Dilution**	**Company**
GAPDH	1:10000	Merck / Sigma-Aldrich
BRAF	1:1000	R&D systems
RAF1	1:1000	R&D systems
p-ERK1/2	1:1000	R&D systems
TGFBR1	1:1000	CUSABIO
ITCH	1:1000	
p-SMAD2/3	1:1000	
Smurf2	1:1000	NOVUS

Secondary antibodies	**Dilution**	**Company**
Goat Anti-Rabbit IgG	1:1000	BIOSS
Goat Anti-Mouse IgG	1:000	BIOSS

Supplementary Figure 1. Venn-diagrams of BRAF and double mutant EV-enriched miRNAs

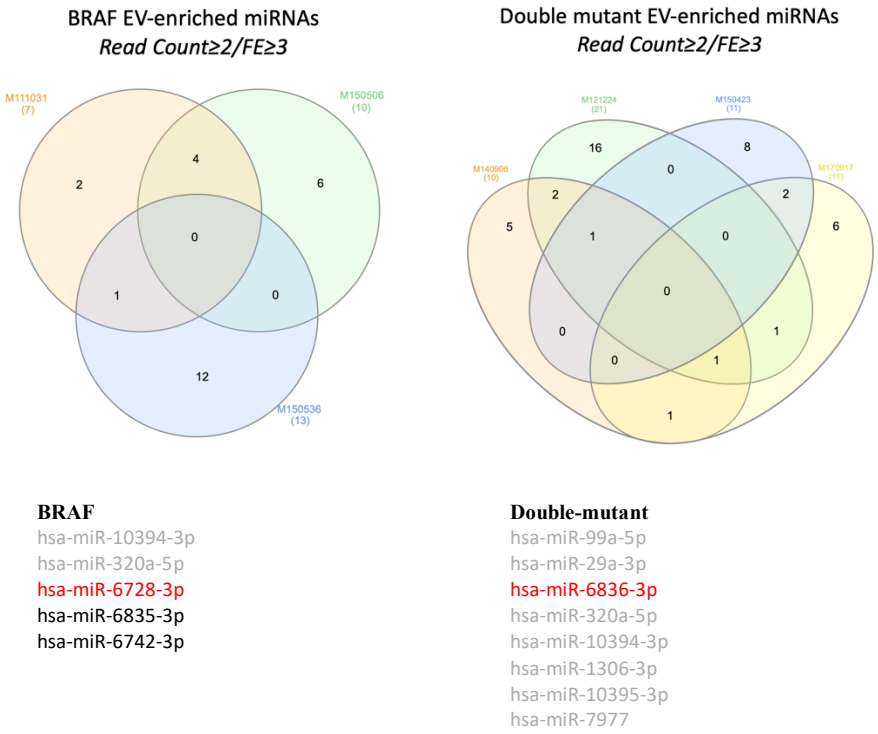

BRAF
hsa-miR-10394-3p
hsa-miR-320a-5p
hsa-miR-6728-3p
hsa-miR-6835-3p
hsa-miR-6742-3p

Double-mutant
hsa-miR-99a-5p
hsa-miR-29a-3p
hsa-miR-6836-3p
hsa-miR-320a-5p
hsa-miR-10394-3p
hsa-miR-1306-3p
hsa-miR-10395-3p
hsa-miR-7977

Supplementary figure 1. BRAF and Double Mutant shared EV-miRNAs. Left, Venn-diagram showing the BRAF cell lines EV-enriched miRNAs. Right, Venn-diagram showing the double mutant cell lines EV-enriched miRNAs. Tables below indicate the miRNAs that are shared between at least two cell lines. miRNAs that were also expressed in other cell lines are highlighted in Grey. The selected signature miRNA is highlighted in Red. Other candidate miRNAs are highlighted in black. For mutant BRAF, hsa-mir-6728-3p is selected and for double mutant hsa-mir-6836-3p is selected.

Supplementary Figure 2. Target prediction analysis of candidate signature miRNA hsa-mir-6728-3p

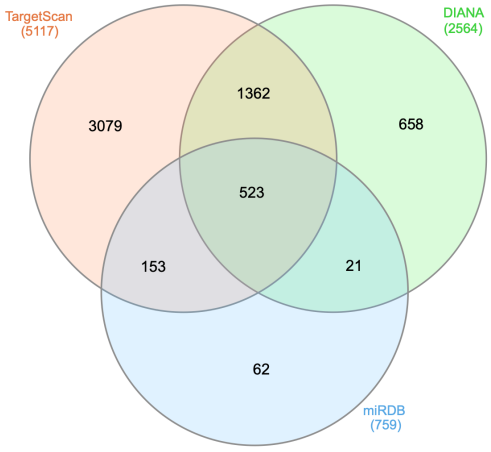

Supplementary figure 2. Target prediction for hsa-mir-6728-3p comparing three free online available tools. TargetScan, DIANA, and miRDB were used to predict targets for hsa-mir-6728. The 523 shared targets were used for gene set enrichment analysis.

Supplementary Figure 3. hsa-mir-6728-3p antagomir treatment does not affect cell viability and drug resistance in M150506

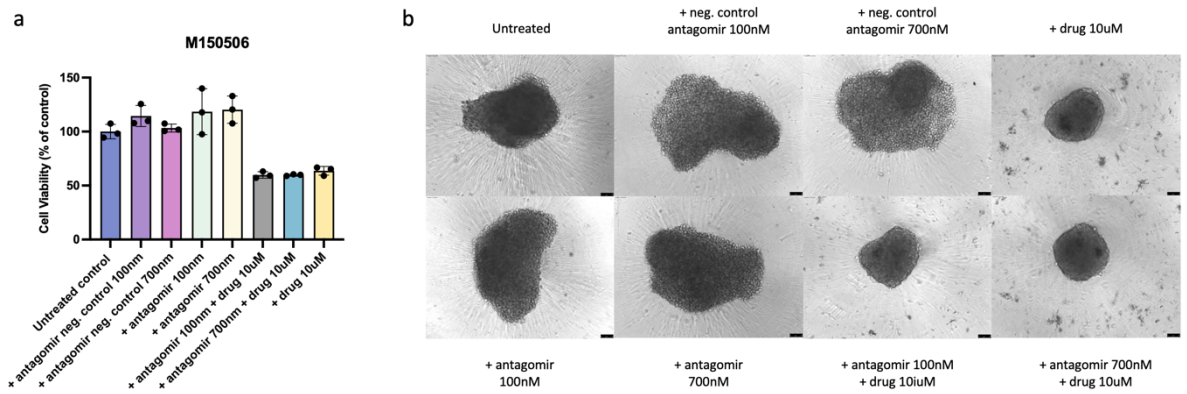

Supplementary figure 3. hsa-mir-6728-3p antagomir treatment does not affect cell viability and drug resistance in M150506. a) The effect of antagomir treatment for hsa-mir-6728-3p on Vemurafenib drug resistance and cell viability for spheroids of M150506. Cell viability is expressed as percentage of control. Spheroids were treated with either 100nm or 700nm of a negative control antagomir or antagomir for hsa-mir-6728-3p with or without 10uM Vemurafenib. SD is indicated by the error bars; n=3. b) Representative bright field images (10X) for all conditions at day 6 of M150506 spheroids. Scale bar represents 75um.

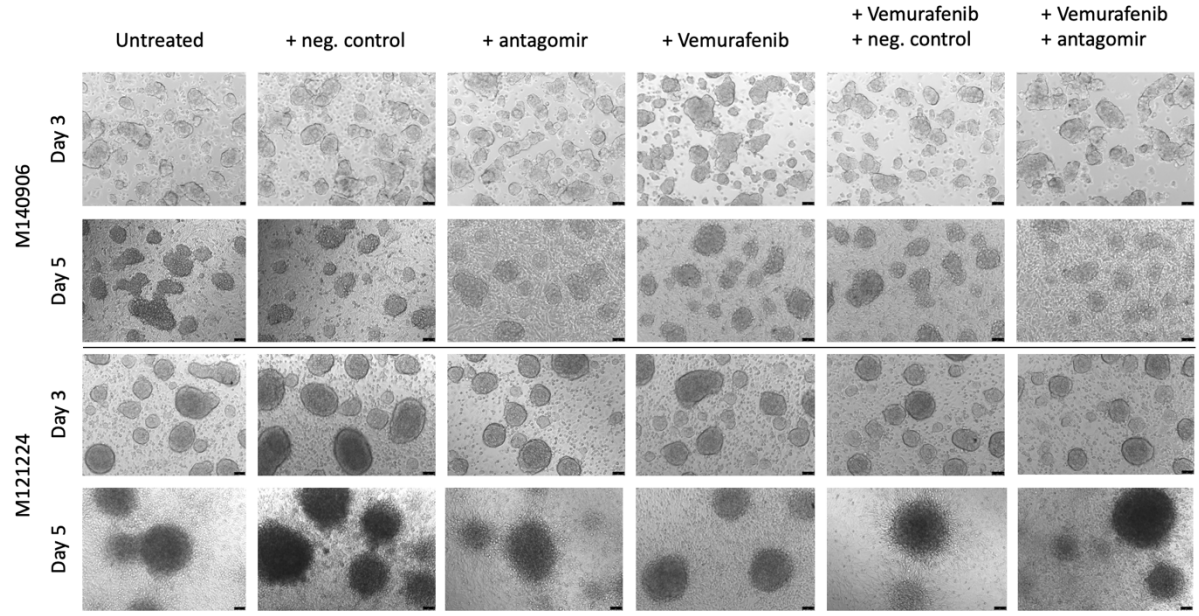

Supplementary figure 4. hsa-mir-6836-3p antagomir treatment does not affect morphology in double mutant spheroids. Representative bright field images (10X) for all conditions at day 3 (before treatment) and day 5 (after treatment) for M140906 and M121224 are shown. Scale bar represents 75um.